University of Bristol - Explore Bristol Research
General rights

Highlights

➢ Five sets of submerged marine terraces have been recognized at different depth on Santa Maria's insular shelf.

➢ The possible correlation between the formation of raised and submerged terraces with relative sea-level changes have been investigated.

➢ The presently raised marine terraces were probably formed from ~3.5 Ma to ~1 Ma, whilst submerged terraces were formed from ~1 Ma to the Last Glacial Maximum.

➢ A better estimation of the uplift trend for Santa Maria island has been proposed.

➢ The formation and preservation of marine terraces is discussed according to a number of interacting factors.

Marine terrace development on reefless volcanic islands: new insights from high-resolution marine geophysical data offshore Santa Maria Island (Azores Archipelago)

Alessandro Ricchi[1], Rui Quartau[2,3]; Ricardo S. Ramalho[3,4,5]; Claudia Romagnoli[1]; Daniele Casalbore[,6,7]; João Ventura da Cruz[2]; Catarina Fradique[2]; André Vinhas[2]

[1] University of Bologna, Dip. Scienze Biologiche, Geologiche e Ambientali, Bologna, Italy

[2] Instituto Hidrográfico, Divisão de Geologia Marinha, Lisboa, Portugal

[3] Instituto Dom Luiz, Faculdade de Ciências, Universidade de Lisboa, 1749-016 Lisboa, Portugal

[4] School of Earth Sciences, University of Bristol, Wills Memorial Building, Queen's Road, Bristol, BS8 1RJ, UK

[5] Lamont-Doherty Earth Observatory at Columbia University, Comer Geochemistry Building, PO Box 1000, Palisades, NY10964-8000, USA

[6] Sapienza Università di Roma, Dipartimento Scienze della Terra, Roma, Italy

[7] Istituto di Geologia Ambientale e Geoingegneria, Consiglio Nazionale delle Ricerche, Area della Ricerca, Roma, Italy

*Corresponding author: alessandro.ricchi7@unibo.it (Alessandro Ricchi)

1

ABSTRACT

Submerged marine terraces are relict coastal erosional landforms now underwater due to rising sea level and/or land subsidence. Using as case study the shelf around Santa Maria Island (North Atlantic Ocean), we intend to advance our knowledge of the formation and preservation of these features on reefless volcanic islands. Santa Maria is an ideal place to study their combined generation, since it displays a sequence of subaerial and submerged marine terraces (the latter not studied before), distributed between 7/230 m in elevation, and -40/-140 m, respectively. Based on some geological constraints, we investigated a possible correlation between the formation of the different terraces with known sea-level changes. Our results suggest that the spatial distribution of marine terraces at Santa Maria depends on the complex interplay between glacio-eustatic sea-level fluctuations, the island's vertical motion trends, the morphology of the shelf, and the intensity of marine erosion. Subaerial terraces probably developed from ~3.5 Ma to ~1 Ma following a fortuitous conjugation of optimal exposure to energetic waves and a suitable arrangement/lithology of the stratigraphic units promoting easier erosion. Their preservation was likely promoted by the uplift trend the island experienced in the last 3.5 Ma, which was rapid enough to prevent their destruction by subsequent highstands. The submerged terraces, presumably all younger than ~1 Ma, were largely influenced by shelf gradient, leading to more developed and preserved terraces in wider and low-gradient sectors. Displacement by active faults also conditioned the formation and further development of both subaerial and submerged terraces, with tectonic activity documented for the 0.693 Ma -2.7 Ma period.

1. INTRODUCTION

3

Relative sea-level changes have left unambiguous morphologies in the geological record, as attested by the presence of coastal notches (e.g. Ferranti et al., 2006; Trenhaile, 2015), marine terraces (e.g. Zazo et al., 2002, Pedoja et al., 2014) and beach rocks (e.g. Mauz et al., 2015). In submarine settings the effects of glacio-eustatic sea-level changes can be witnessed by markers such as the shelf breaks on insular shelves (Quartau et al., 2014) or depositional features formed below storm-wave base (e.g. submarine prograding wedges; Casalbore et al., 2017a and references therein). Marine terraces are frequently referred to as excellent tracers of palaeo sea-level (Pirazzoli et al., 1993) and they can be used to discern the vertical movements affecting the coastline (Campbell et al., 1986; Ferranti et al., 2006; Zazo et al., 2007). This approach has been successfully applied to study the history of uplifting volcanic islands, (see Lucchi et al., 2007; Lucchi, 2009 and Ramalho et al., 2017) where vertical deformations usually operate at varied timescales (De Guidi and Monaco 2009; Ramalho et al., 2013). Most studies so far did not integrate the offshore information (Quartau et al., 2013; 2015), and when they did, mostly focused on oceanic islands surrounded by coral reefs (Coulbourn et al., 1974; Blanchon and Jones, 1995; Faichney et al., 2010). To date, only few studies have looked closely at submerged terraces on reefless volcanic islands or at seamounts (Passaro et al., 2011; Schwartz et al., 2018) and consequently little is known about the factors that control the generation and timing of submerged terraces in these settings.

Santa Maria is the southeastern-most and oldest island of the Azores Archipelago in the Atlantic Ocean, with a history of intermittent volcanism spanning between approximately 6 to 2.8 Ma (Sibrant et al., 2015a; Ramalho et al., 2017). Its subaerial evolution is now well constrained (Serralheiro et al., 1987; Serralheiro, 2003; Ávila et al., 2008; Sibrant et al., 2015a; Ramalho et al., 2017) and so is the history of vertical movements affecting the island edifice. Based on several volcanic, erosional, and sedimentary relative sea-level markers found onshore, Ramalho et al.

4

68   (2017) inferred that Santa Maria was subjected to over 200 m of subsidence from emergence at 6

69   Ma until 3.5 Ma BP (at average ~100 m/m.yr.), after which the island experienced an uplift trend

70   at a slower pace (~60 m/m.yr. on average) until recent times. Additionally, Ramalho et al. (2017)

71   reported a sequence of subaerial marine terraces at elevations ranging between 7-11 m and 210-

72   230 m, formed during the post-erosional stage of the island. In this paper, the analysis of newly

73   acquired high-resolution multibeam bathymetry and seismic profiles reveal a sequence of

74   submerged marine terraces extending to the shelf edge. This makes Santa Maria an ideal case

75   study to employ a combined onshore/offshore approach to investigate the generation of subaerial

76   and submerged marine terraces and their likely timing of formation in relation to the island's

77   vertical motion history. Based on one dated subaerial terrace and a dated passage zone between

78   subaerial and submarine lava flows (which were used as "anchor" points), we also present a

79   possible correlation between each subaerial and submerged terrace identified on the island and

80   their respective possible time of formation, as extracted from published eustatic curves. The case

81   study of Santa Maria therefore will improve our understanding of the controlling mechanisms of

82   marine terrace formation and preservation at reefless volcanic islands, and more generally in

83   other settings.

84

85   *2. GEOLOGICAL BACKGROUND*

86   The Azores Archipelago consists of a group of nine volcanic islands in the mid-North Atlantic,

87   located around the triple junction between the North American, Eurasian and Nubian lithospheric

88   plates (Fig. 1). The Eastern (São Miguel and Santa Maria) and Central group of islands (Terceira,

89   Graciosa, São Jorge, Pico, and Faial Islands) are located on a roughly triangular-shaped area

90   between the Terceira Rift (TR in Fig. 1) and the inactive East Azores Fracture Zone (EAFZ in Fig. 1)

91   on the eastern side of the Mid-Atlantic Ridge (MAR in Fig. 1; Lourenço et al., 1998; Gente et al.,

92   2003; Miranda et al., 2018). This complex volcano-tectonic structure is the result of a right-

93   transtensional shear zone that links the MAR with the Gloria Fault (GF) (Hipólito et al., 2013;

94   Lourenço et al., 1998; Marques et al., 2013). Santa Maria Island is considered now outside the

95   influence of such wide structure after a ridge-jump, occurred at ~4 Ma, from the incipient Princess

96   Alice Rift (PAR in Fig. 1) to the present-day Terceira Rift (Miranda et al., 2018).

97   Santa Maria was the first island in the Azores Archipelago to emerge above sea level, at

98   approximately 6 Ma (Ramalho et al., 2017). The present-day edifice rises from the -2500 m isobath

99   to a summit at 587 m (Pico Alto, Fig. 2). The emergent stage of island building corresponds to the

100   Cabrestantes and Porto Formations, which crop out on the western side of the island (age ~6 Ma,

101   Fig. 2a). Then, a subaerial shield volcano was formed about 5.8 – 5.3 Ma, which consolidated the

102   island edifice (Anjos Volcanic Complex, Fig. 2a). During the following ~1 Ma, volcanic activity

103   waned, leading to a partial or complete dismantling of the shield volcano and to marine deposition

104   synchronous with occasional, low-volume submarine volcanism (Touril Volcano-sedimentary

105   Complex, Fig. 2a). This stage is considered as mainly erosional and occurred alongside a significant

106   subsidence trend, which further contributed to the planation and possibly complete submergence

107   of the island edifice (Ramalho et al., 2017). At ~4.1 Ma, however, renewed volcanic activity, which

108   culminated in the creation of the Pico Alto Volcanic Complex (Fig. 2a), caused the edifice to re-

109   emerge, as attested by the vertical succession of submarine and subaerial volcanic products. At

110   ~3.5 Ma subsidence reversed into uplift, as attested by the presence of raised submarine volcanic

111   sequences and a succession of subaerial marine terraces on the western (windward) side

112   (Ramalho et al., 2017), arranged in a typical staircase morphology. Conversely, the eastern

113   (leeward) side is characterized by a rugged morphology, featuring high plunging cliffs (up to 250-

114   300 m in elevation) with occasional wave-cut notches at varying elevations. A last stage of

115   volcanism (3.2-2.8 Ma) created the Feteiras Formation (Fig. 2a), but this activity did not reverse

6

116   the dominantly erosional trend the island has experienced in the last 3.5 Ma (Ramalho et al.,

117   2017).

118   In terms of tectonics, Santa Maria is mainly dominated by NW–SE-, N-S and NE–SW-trending

119   extensional faults (Madeira et al., 2015), as attested by the existence of main morphological

120   lineaments in the subaerial topography that displace some of the subaerial terraces (Fig. 2a;

121   Madeira et al., 2015). Numerous dikes, contemporaneous with the two main shield building

122   stages, striking N 045° and N 150° have also been reported (Zbyszewski and Ferreira, 1960;

123   Serralheiro et al., 1987) (Fig. 2a).

124   In the Azores Archipelago the wave regime is dominated by waves impacting the coastline from

125   the NW (29%), W (24%) and N (16%), with average significant heights (H_s) ranging between 2.5 m

126   and 3 m (Quartau et al., 2012). Storminess in the Azores is high, and the archipelago is struck by

127   severe storms, at least once every seven years (Andrade et al., 2008) that are able to produce

128   maximum wave heights up to 20 m (Rusu & Guedes Soares, 2012). The Azores is subjected to

129   semidiurnal regular tides and the annual mean tidal range in Santa Maria Island is about 1,44 m

130   (Instituto Hidrográfico, 2000).

131

132   *3. DATA AND METHODS*

133   *3.1 MARINE GEOPHYSICAL DATA ACQUISITION*

134

135   High-resolution multibeam bathymetric and seismic reflection data were collected around

136   Santa Maria between -20 m and -250 m onboard the R/V *Arquipélago* from 24th August to 15th

137   September 2016.. High-resolution multibeam bathymetry was collected mostly parallel to the

138   isobaths along overlapping track lines, relying on DGPS with OMNISTAR corrections for positioning

139   and using a pole-mounted Kongsberg EM2040C™ system (operating frequency range of 200-400

7

KHz and angular coverage of 130°). Sound velocity profiles (SVP, yellow dots, fig. 3) were regularly

collected during the survey. Data were processed using Caris Hips & Sips 9.0 software to produce

high-resolution Digital Elevation Models (DEMs) with variable cells size depending on the water

depth (1 m for shallow water to 8 m at ~250 m).

A total of 2008 km of high-resolution seismic profiles (Fig. 3) was also acquired between -25 m

and -300 m using an Applied Acoustic Engineering AA 200 Boomer™ plate and a receiver array

consisted of a single-channel streamer with 8 hydrophones. Most of the seismic profiles were

acquired using 100/200 J of output energy, depending on the water depth. Seismic survey lines

parallel to bathymetry have line spacing varying with depth (between 20 to 200 m), while seismic

lines perpendicular to the coastline were regularly spaced at ~250 m.

3.2 TERRACE MAPPING

Multibeam bathymetry and seismic profiles were combined with an existing onshore

topographical model (generated from a 1:5000 scale digital altimetric database) in a GIS

environment, allowing for integrated onshore/offshore geomorphological analysis. Using this

database, we mapped the erosive shelf edge and the submerged terraces on the shelf. Specifically,

we mapped (where possible) the inner margin of each terrace (Fig. 4, also named "shoreline

angle"), which provides an estimation of the shoreline position at the time it was formed, within

an error of few meters (Firth et al., 1996; Trenhaile, 2002; Antonioli et al., 2003). Where the shelf

and overlying terraces are covered by sediment, we used seismic profiles to measure their

extension and edge depth. In such cases a sound velocity of 1800 m/s was adopted for the

time/velocity conversion for sediments, which on the Azorean mid/outer shelves often correspond

to sands (Quartau et al., 2012).

164   The mapped shelf was divided into four sectors (north, west, south, east), based on their

165   orientation to the wave climate, their distinctive morphology and the distribution of submerged

166   terraces (Figs. 5, 7-10; 3 and 8 on the Electronic Supplementary Material, hereafter ESM). To

167   consider the island vertical movements, we always took into account the maximum values of the

168   shelf edge depths for each sector, since later retrogressive erosion might have affected its depth,

169   making it shallower in places. Mean values of the terrace width were calculated from bathymetric

170   profiles plotted every 250 m perpendicular to the coastline and/or the shelf edge (Fig. 8ESM). The

171   width of the subaerial terraces was also measured using topographic profiles (Fig. 8ESM and Table

172   3ESM) to obtain average values, assuming that it corresponds to the distance from one

173   palaeoshoreline to the one immediately above or below.

174

175   *3.3 ESTIMATE OF THE AGE OF SUBAERIAL AND SUBMERGED MARINE TERRACES*

176

177   The uplift rates of Santa Maria were calculated using two dated subaerial markers,

178   together with published sea-level curves. Considering the time period under analysis (almost 4

179   Ma) we merged the Bintanja and Van de Wal (2008)'s curve, which has a very good resolution and

180   covers 3 Ma, with a curve having a lower resolution (De Boer et al., 2010) for periods after 3 Ma

181   (Fig. 6).

182   The subaerial marine terrace at 90 m above sea level (a.s.l.; dated at 2.15±0.03 Ma, Ramalho et al.,

183   2017) and the maximum highstand between 2.12 Ma and 2.18 Ma (-0.47 m at 2.134 Ma) were

184   used as reference markers to calculate the possible uplift rate to recent times, assuming that

185   during that period this terrace was uplifted from -0.47 m to 90 m a.s.l.. Using this methodology,

186   we obtained an average uplift rate of 42.4 m/m.yr (0.042 mm/yr). The passage zone between

187   subaerial and submarine lava flows of the effusive lava deltas of Monte Gordo (Fig. 2a) was chosen

9

188   as another reference sea-level marker to calculate an earlier uplift trend. This feature, that marks

189   very accurately the position of sea level at the moment of the eruption (e.g. Cas and Wright, 1987;

190   Porebski and Gradzinski, 1990; Ramalho et al., 2010a,b,c; Ramalho, 2011; Meireles et al., 2013), is

191   located at 190 m a.s.l. and its timing of formation is constrained by two ^{40}Ar/^{39}Ar analyses (SMA 18

192   and SMA 45 samples collected in the submarine lava flows below the passage zone) yielding ages

193   of 3.63±0.09 and 3.71±0.08 Ma (see Ramalho et a., 2017). Although the formation of this lava

194   delta did not occur, necessarily, during a highstand, the temporally nearest highstand provides a

195   minimum value for the inferred vertical displacement experienced by this marker, which

196   constitutes the highest datable sea-level indicator in Santa Maria (Ramalho et al., 2017). The

197   average age of the marker is 3.67 Ma, which falls between two highstands in our composite curve.

198   Therefore, we used the nearest and highest highstand (dated as 3.704 Ma, at 6.4 m above present

199   sea-level) to calculate the average uplift rate, which is approximately 59 m/m.yr (0.059 mm/yr).

200   The result is an uplift rate that progressively slowed down with time, in agreement with the

201   current elevation of the Marine Isotope Stage (MIS) 5e raised terrace (7-11 m a.s.l.), which attests

202   to a substantial vertical stability, or to very small uplift, on Santa Maria Island in the last 125 ka.

203   The composite sea-level curve, based on the literature, has been modified according to the

204   obtained uplift rates (Fig. 6), in order to infer the possible age of formation of the mapped marine

205   terraces. Accordingly, we tentatively matched all the stands (including highstands, stillstands and

206   lowstands) and all the passing sea-level cycles (rises and falls) with the current terrace

207   elevation/depth (see section 4.3). We assumed that subaerial and submerged marine terraces

208   could be multi-generational, i.e. their geometry could result from the action of several stillstands,

209   as well as sea-level passages. We are, in fact, aware of the inherent errors of using one sea-level

210   curve in detriment of another (Caputo, 2007) and also that uplift rates have possibly changed

211   through time in the period of our reconstruction (Ramalho et al., 2010b). Although a confident

10

correlation between a particular terrace and a single sea-level stand is impossible, the establishment of a probable time frame for its likely formation can be proposed. Moreover, we also took into account the time that waves eventually would take to carve the terraces at a specific depth, within a ±5 m uncertainty (i.e, we considered for the calculations the timing that sea was 5 m above and below the level of the terrace) (see Table 1ESM).

4. RESULTS

4.1 THE INSULAR SHELF AROUND SANTA MARIA ISLAND

The northern sector of the shelf (Fig. 7) has a rough trapezoidal shape, being widest in front of Ilhéu das Lagoinhas (~8 km) and narrower westwards (~4.5 km). The northwestern-most tip of the shelf is characterized by an oval-shaped, 200 m-high conical structure (Baixa do Ambrósio) that likely represents the remnants of an old pillow-lava cone. Other concentric structures, probably corresponding to truncated cinder/scoria cones of the Cabrestantes and Porto Formations, and of the Anjos Volcanic Complex have been also identified, mostly on the easternmost portion from -120 m to -30 m. The westernmost portion of the inner shelf is divided into three rocky blocks by sharp and linear escarpments (2 to 2.5 km long, Fig. 7) that are, apparently, the seaward expression of tectonic lineaments recognized on land (Aeroporto, Anjos and Baía da Cré faults in Figs. 2 and 7). The shelf edge depth is constantly below -125 m with maximum depths of ~-170 m to NW off Baía do Mar da Barca (Fig. 7).

The western sector of the shelf is generally characterized by a rocky surface with almost no sediment cover. A WNW-ESE lineament located offshore Campo Grande (possible fault, Fig. 8), separates the shelf into two parts characterized by different widths (~1 km to the north, ~2 km to

235 the south). In this sector the erosive shelf edge has been significantly affected by mass wasting;

236 where preserved, its depth varies between -100/-110 m to -135/-145 m (Fig. 8).

237   The southern shelf sector has an irregular morphology, since more preserved and wider

238 portions of the shelf alternate with narrower areas affected by gully heads (Fig. 9). Accordingly,

239 the shelf width varies from ~0.7 km to up to ~2.5 km and the edge depth from -80/-90 m to a

240 maximum value of -142 m (Fig. 9). Sharp NNE-SSW oriented lineaments cut the shelf, often

241 defining rocky structural highs, which are bordered by more depressed areas covered by

242 sediments (Fig. 9).

243   The eastern sector of the shelf is from ~1 to ~2 km wide, with the erosive shelf edge located at

244 a fairly constant depth, varying mostly between -90 m and -110 m (Fig. 10). Some portions of the

245 outer shelf are affected by landslides which contributed to a decline in the shelf width and the

246 depth of its edge. The morphology of the shelf is generally rough and thus associated with rocky

247 outcrops alternating with patchy sedimentary cover, similar to the southern sector.

248

249 *4.2 SUBMERGED MARINE TERRACES*

250

251 Five sets of marine terraces, with their inner margins located approximately at -40/-50 m, -70/-80

252 m, -85/-90 m, -100/-110 m and -120/-140 m were identified on the shelf around Santa Maria (Figs.

253 7 to 14 and Figs. 1ESM to 7ESM).

254

255 *4.2.1 Terrace at -40/-50 m*

256   This terrace is marked by an inner margin generally located between -40 m and -50 m (black

257 line in Figs. 7-10, 12-14, and 4ESM-7ESM), while the outer edge depth varies between -50 m and -

258 60 m. Overall, this terrace exhibits a patchy distribution on the northern sector and is narrow

12

259   (~400 m, Fig. 7 and Table 2ESM) when compared to other terraces and to the shelf extent in the

260   north. This terrace is ~200 m wide along the western shelf sector (Table 3ESM) extending to ~300

261   m and ~400 m, respectively, along the southern and the eastern shelf sectors; it is wider than the

262   remaining terraces on the western, southern and eastern shelf sectors (Figs. 9, 10, 16 and Table

263   2ESM). The terrace is laterally discontinuous as it is interrupted by tectonic lineaments in the

264   northern and western shelf sectors (respectively offshore Baía do Mar da Barca-Baía da Cré and

265   Campo Grande, Figs. 7 and 8) and is compartmentalized by rocky blocks in the southern and

266   eastern sectors (Figs. 9 and 10).

267

268   *4.2.2 Terrace at -70/-80 m*

269   The terrace with an inner edge located at -70/-80 m is evident in almost the entire northern

270   shelf sector and on the summit of the pillow cone of Baixa do Ambrósio (blue line in Figs. 7-10, 12-

271   14 and 2ESM, 4ESM-7ESM). This terrace is up to ~2 km wide (average width of ~880 m, Table

272   2ESM) along the easternmost portion of the northern shelf. To the west (corresponding to the

273   rocky blocks offshore Ponta dos Frades, Fig. 7) its expression is markedly reduced, having the same

274   discontinuous nature as the terrace at -40/-50 m. Despite being less extensive and being partly

275   eroded by small landslides, the same terrace is evident on the western shelf sector to the north of

276   the WNW-ESE trending tectonic lineament offshore Campo Grande (average width of 100 m, Fig. 8

277   and Table 2ESM). South of this lineament it is almost absent. Along the southern shelf sector, this

278   terrace is interrupted by tectonic lineaments, being mainly developed offshore Ponta do Castelo

279   (~300 m wide, Fig. 9). Here the average width is about 90 m (Table 2ESM). Along the eastern shelf

280   sector, the terrace occurs discontinuously (Fig. 10) and is ~100 m wide on average (Table 2ESM).

281

282   *4.2.3 Terrace at -85/-90 m*

13

283   This terrace has an inner edge located at -85/-90 m (yellow line in Fig. 7, 9, 10, 1ESM, 4ESM-

284   7ESM) being wider in the northern shelf sector (Fig. 7), where it can attain widths of ~ 1 km (over

285   500 m on average, Table 2ESM). Along the rocky outcrops offshore Ponta dos Frades, it is also

286   interrupted (like the two previous terraces) by lineaments. Apart from the northern shelf sector,

287   this terrace is also preserved in places along the southern sector (average width of 50 m, Table

288   2ESM), where it is also partly interrupted by tectonic lineaments (Fig. 9). Along the eastern sector

289   it occurs sporadically with an average width of 50 m (Fig. 10 and Table 2ESM).

290

291   *4.2.4 Terrace at -100/-110 m*

292   This terrace has an inner edge located at -100/-110 m (purple line in Figs. 7-9, 11-13, 2ESM,

293   4ESM-6ESM) and the greatest width along the northern sector (average 800 m, Table 2ESM),

294   which progressively decreases from west to east. This terrace has also been detected around Baixa

295   do Ambrósio, even if it is narrower (commonly less than 50 m) (Fig. 7). The inner edge also appears

296   to be affected by the faults seen offshore Anjos and Baía da Cré (Fig. 7), although less distinctively

297   when compared with other terraces. Along the western and southern shelf sectors the same

298   terrace is observed in narrow strips where the shelf edge is deeper (Figs. 8, 9, and 4ESM-6ESM)

299   and has average widths of 70 m and 50 m, respectively (Table 2ESM). In these sectors, several

300   landslide scars make the terrace laterally discontinuous (Figs. 8 and 9). This terrace is not present

301   on the eastern shelf sector (Fig. 10).

302

303   *4.2.5 Terrace at -120/-140 m*

304   This is the deepest submerged terrace identified on the shelf, with the inner edge located

305   between -120 and -140 m (red line in Figs. 7-9, 11, 13, 1ESM, 2ESM, 4ESM-6ESM). Along the

306   eastern and central portions of the northern shelf sector it is characterized by a patchy

14

307   distribution, whilst to the west it widens (offshore Anjos to Baía do Mar da Barca in Fig. 7), being

308   characterized by a sub-horizontal surface and an evident inner edge (Fig. 1ESM). This submerged

309   terrace has also been detected at Baixa do Ambrósio (Fig. 7). In the northern sector it has an

310   average width of 300 m (Table 2ESM), whereas it is marked by narrow and discontinuous strips

311   (average widths of ~100 m) affected by small-scale landslide scars on the western shelf sector (Fig.

312   8). Along the southern shelf sector, it is almost absent apart from a sub-horizontal surface, with an

313   inner edge at ~-120 m. The terrace has an average width of ~130 m (Table 2ESM) while its

314   maximum width is ~300 m offshore Ponta do Castelo (Figs. 9 and 13). This terrace is also absent

315   along the eastern sector (Figs. 10 and 14).

316

317   *4.3 CORRELATION OF MARINE TERRACES WITH SEA-LEVEL OSCILLATIONS*

318

319   Following the approach described in section 3.3, and taking into account the associated

320   limitations and uncertainties, a possible timeframe for the formation of each marine terrace is

321   here proposed (Fig. 15). It was assumed that the subaerial terraces were preserved when uplift

322   quickly carried them above the level of wave action (see Trenhaile, 2002 and 2014). Because of

323   uplift, only the most recent sea-level stands could be responsible for the formation of the

324   submerged terraces. The results of our reconstruction (Fig. 15) imply that the uppermost subaerial

325   terrace (210/230 m a.s.l.) recognized by Ramalho et al. (2017) has no match with sea-level stands

326   younger than 3.5 Ma. This is largely a modeling artifact given that we anchored the formation of

327   the Pico Alto lava deltas to a particular highstand at 3.704 Ma. Moreover, the 210/230 m terrace

328   was marked by Ramalho et al. (2017) with a high uncertainty because its morphologic imprint on

329   the island is not clearly recognizable. Given these limitations, we will focus our analysis on terraces

330   that are located below the passage zone of Pico Alto's lava deltas (at approximately 200 m). These

15

terraces can be found down to 45/50 m in elevation, after which the island is cliff-bounded, with no visible terraces excepting the 7–11 m terrace, which is preserved in places (see Fig. 5). Accordingly, we propose that the subaerial marine terraces (with the exception of the lowest and highest) were formed between 3.436 Ma to 1.065 Ma BP (Fig. 15 and Table 1 ESM). The lowest subaerial terrace (7-11 m), despite being exclusively attributed to MIS 5e by Ramalho et al. (2017) on the basis of existing sedimentary deposits, according to our model could have been formed and subsequently modified from 1.749 Ma to 121 ka (a period of 1.628 m.yr., Table 1ESM). Our reconstructions also suggest that, on account of the reduction of uplift trend but also because of the gradual increase in the amplitude of the sea-level oscillations, as well as a decrease in their frequency, from 2.8 Ma to the present, the possible age interval during which sea level was able to carve and modify these terraces also increased (Fig. 15). Using the same approach, the formation and subsequent development of the submerged terraces probably took place in various stages between 1.122 Ma and 12.1 ka, with the deepest submerged terrace (-120/-140 m) being only affected by the lowstand at 19.8 ka (MIS 2; Table 1ESM).

A parameter to consider in these reconstructions is also the effective time that sea level was at a particular elevation to form a terrace (within a ±5 m uncertainty; see Table 1ESM). This is different from the possible age interval during which sea level passed through each terrace elevation i.e., considering also the combined effects of uplift and glacio-eustatic oscillations. Whilst the possible age interval for the formation of a terrace provides us with a maximum and minimum age for that terrace, the effective time quantifies the actual amount of time sea level spent at that particular elevation. This information provides the total amount of time a terrace was effectively exposed to active wave erosion during all the cycles included within the possible age interval. For instance, the effective time during which sea level was at the elevation of the inner margin of the 45/50 m raised terrace (305 k.yr.) is estimated to be similar to that of the 155/165 m terrace (318.7 k.yr.)

16

355   although the possible age interval for their formation is very different (respectively 1.460 m.yr.,

356   i.e. between 2.525 Ma and 1.065 Ma, and 373 k.yr., i.e. between 3.436 Ma and 3.063 Ma, Table

357   1ESM).

358

359   *5. DISCUSSION*

360

361   Several geological and oceanographic factors – such as uplift/subsidence rates, local

362   changes in wave regime, shelf gradients, differential resistance to erosion, amplitude of sea-level

363   oscillations and stillstand duration – influence the formation and preservation of marine terraces

364   (Trenhaile, 2002, 2014; Ramalho et al., 2013). It is thus difficult to isolate, in quantitative terms,

365   the contribution of each of these factors in controlling the spatial distribution of the observed

366   terraces.

367   Our correlation between the present-day position of marine terraces and relative sea level

368   for the last 3.5 Ma allowed us to suggest a likely timing (or age interval) of formation for each

369   subaerial and submerged terrace. Despite the many sources of uncertainty in this approach – such

370   as uncertainties in the adopted eustatic curve (particularly before the last 3 Ma) and in uplift rates,

371   along with the fact that we did not incorporate any effects of glacio-isostatic adjustment –it

372   constitutes a first-order approximation from which useful insights can be derived concerning the

373   generation, destruction, and preservation of marine terraces along an uplifting landmass,

374   throughout a considerable period of time (3.5 m.yr.) and under the effects of multiple glacio-

375   eustatic cycles. This integrated onshore/offshore approach has been rarely adopted but

376   constitutes the basis for a more complete, holistic comprehension of how long-term relative sea-

377   level change interacts with landmasses to form distinctive coastal and nearshore morphologies

378   such as subaerial and submerged terrace staircases.

17

379

5.1 SUBAERIAL TERRACES

381

According to Ramalho et al. (2017), the interplay between exposure to the dominant wave direction (from the western quadrant, i.e. the windward side) and a favorable lithological/stratigraphical framework (i.e. the softer Touril sequence and the gently dipping contacts between this units and underlying Anjos and overlying Pico Alto volcanic edifices) in the western half of Santa Maria, enhanced coastal retreat and formed a wide and gently-sloping terraced morphology, under the combined action of uplift and glacio-isostatic oscillations. We agree with this model, which offers a simple-enough explanation for the island asymmetry, being in tune with the local lithological, structural, and oceanographic conditions. Our analysis, however, suggests that the effective time of formation is also an important factor contributing to the generation of the terraced morphology in this part of the island, and to the greater width of the terraces now located between 50 m and 120 m in elevation.

Our reconstructions suggest that subaerial terraces at Santa Maria are most probably polygenic because uplift rates were low enough to expose each terrace to the passage of several sea-levels (Fig. 15). As such, these terraces were affected by wave erosion during multiple cycles of rising and falling sea level (Fig. 15, Table 1ESM). According to our calculations, the effective time that each terrace was exposed to wave erosion with passing sea level spans from ~140 to ~319 k.yr., much more than the average duration of a single highstand or stillstand. A possible relationship exists between terrace width and effective time, e.g. wider terraces were subjected to marine erosion for longer time periods. The plot between terrace width vs effective time shown in Fig. 16 (see also Tables 1ESM and 3ESM) suggests a positive correlation between these two parameters, with terrace width increasing proportionally to the effective time they have been exposed to sea level.

18

Notable exceptions to this trend include the 105–110 m and 155–165 m terraces, which are considered outliers for different reasons. The 105–110 m terrace coincides with the bulk of the softer Touril sequence (allowing for enhanced coastal retreat in a shorter period of time) and therefore it is not surprising it deviates from this relationship. Why the 155–165 m terrace is relatively narrow despite the fact it was probably exposed for a longer effective time (Table 3ESM) is more difficult to explain. However, a possible explanation lies in the fact that this terrace, being one of the oldest, has suffered considerable topographic decay since its formation.

A peculiar fact about Santa Maria is that it does not exhibit any well-developed raised marine terraces below 45-50 m in elevation, with the exception of the 7–11 m terrace, attributed to MIS 5e (Ramalho et al. 2013; Ávila et al. 2015c; Ramalho et al. 2017). In between these elevations, only rare and poorly-developed wavecut notches can be observed (Ramalho et al., 2017). In our view, the combined effect of two factors might have contributed to this absence. One is related to the fact that in the last 1 m.yr. the frequency of the glacio-eustatic oscillations started to be dominated by the longer 100 k.yr. (Miller et al. 2005), reducing the effective time for erosion at each elevation over this whole period, as highstands/stillstands were fewer when compared to the Late Pliocene and Early- to Mid-Pleistocene. During the latter period, the amplitude of glacio eustatic oscillations was lower and their frequency was dominated by the 41 k.yr cycles, implying more frequent passages of sea level at each elevation (resulting in longer effective times for erosion). The second effect could be related to a slowdown in uplift rates – perhaps a slowdown even more dramatic than we modelled in Fig. 15 – during which terrace preservation would be significantly inhibited, with erosion at each subsequent highstand erasing previous terraces and contributing to the maintenance of steep plunging cliffs. This reduction in uplift rates is, in fact, supported by the position of MIS 5e deposits and notches, which indicate a relative sea-level at 7–11 m, a position just slightly above the expected elevation for MIS 5e in the area (Bintanja and Van

19

427   de Wal., 2008). Our reconstructions suggest that the 7-11 m erosive surface is probably polygenic,

428   notwithstanding the fact that MIS 5e deposits can be found resting on this surface (Callapez and

429   Soares, 2000; Ávila et al., 2008; Ávila et al., 2015c; Ramalho et al., 2017). Fig. 15 shows that in the

430   last 1.7 m.yr multiple stillstands could have effectively contributed to the erosion of such a

431   surface, although this terrace had mantained a significant morphological and depositional imprint

432   by the Last Interglacial. This highstand was thus responsible for planating even further an already

433   existing terrace (carved during previous cycles), being also responsible for the deposition of

434   fossiliferous beach deposits that can nowadays be found preserved at several sites along this

435   palaeo-shoreline.

436

437   *5.2 SUBMERGED TERRACES*

438

439   The distribution and characteristics of the submerged terraces likely result from the interaction

440   of several factors, which contributed to their formation and preservation or destruction,

441   depending on their position. Particularly, the width of the submerged terraces is thought to be

442   controlled by the carved lithology, shelf gradients, water depth at the time of formation,

443   frequency and amplitude of relative sea-level changes (Trenhaile, 2014).

444   Our data show that submerged terraces (except for the shallowest terrace at -40/-50) are much

445   wider and better preserved in the northern shelf sector than in the other sectors. Moreover, this

446   shelf sector is the only one exhibiting the complete set of submerged marine terraces. This

447   situation can be explained by the low shelf gradients characterizing the northern shelf, which likely

448   allowed for the development of much wider terraces, despite the greater wave attenuation

449   induced by the lower gradients (Trenhaile, 2014). Lithological and structural factors probably also

450   contributed to a greater width of terraces in this sector. The profusion of softer pyroclastic

20

451 structures due to numerous cinder/scoria cones, for instance, may have allowed faster marine

452 erosion and enhanced coastal retreat, resulting in wider terraces. Differently, the poor

453 development or even absence of deeper terraces on the other shelf sectors (Table 2ESM) could be

454 related to the steeper pre-existing shelf gradients on harder effusive substrates, which precluded

455 the development and preservation of wide terraces. Previous studies (e.g. Anderson et al. 1999;

456 Trenhaile, 2014) suggested, in fact, that terrace destruction due to marine erosion during rapidly

457 rising sea levels (such as during glacial terminations) is more effective when shelf gradients are

458 steeper. In addition, it should be considered that deeper terraces could have been erased by

459 retrogressive (landward) erosion of the shelf edge by small-scale mass wasting, as suggested by

460 the morphology of the shelf edge along the western, southern and eastern sectors (Figs. 8, 9 and

461 10). Effectively, along the western and southern sectors, the deepest terraces are only present

462 where the shelf edge is preserved in deeper waters. In the eastern sector only shallow- and mid-

463 terraces are present, because the shelf edge is always shallower than -100 m. Due to its geological

464 structure – composed of eastward-dipping steep foresets of pillow lavas and hyaloclastites of the

465 Pico Alto Volcanic Complex – this sector of the shelf is more prone to landsliding and therefore

466 terraces are less likely to be preserved, particularly at greater depths (Ramalho et al. 2013;

467 Ramalho et al. 2017).

468 We have also verified the possible relationship between submerged terrace width vs effective

469 time of erosion (Fig. 16 and Table 2ESM). The data distribution is more scattered than for subaerial

470 terrace, even if a slightly positive correlation can be visually observed in the plots. This larger

471 scatter can be related to the fact that submerged terraces have been affected by more cycles of

472 erosional modification during subsequent periods of rising and falling sea level, being thus

473 characterized by a less distinctive shape than subaerial terraces (Trenhaile, 2014). Unsurprisingly,

474 due to uplift (even if very slow) and increasing eustatic amplitudes in the Late Quaternary, the -

21

475   40/-50 m terrace is generally the widest, except for the northern sector (Figs 15 and 16). This

476   surface is polygenic, and results from recurrent erosion over a greater time period than other

477   submerged terraces (Fig. 15 and Table 2ESM). Conversely, we do not have a simple explanation for

478   its lower width in the northern shelf sector with respect to the deeper terraces; perhaps the

479   lithology where this terrace was carved was harder in the northern sector. More generally, it is

480   also difficult to explain the similar range of width observed for this terrace in the different sectors,

481   unless to imagine that the controlling factors for its genesis (shelf gradients, water depths and so

482   on) or their interplay were quite constant around Santa Maria at the time of its formation.

483

484   *5.3 TECTONIC CONTROL ON MARINE TERRACES*

485

486   Faulting at Santa Maria clearly affects the subaerial terraces from the shallowest one up to at

487   least the 85/90 m terrace, which means that these faults could have been activated sometime

488   after ~2.7 Ma. However, this might have started before, but due to the subaerial erosion and

489   sediment covering of the faults it is impossible to verify. Since the faults also affect the distribution

490   and geometry of the submerged terraces (at least down to the -85/-90 m terrace), according to

491   our model these faults might have been active up to at least 693 ka ago, or 15 ka at the latest. In

492   detail, on the northern shelf sector the shallowest terrace (-40/-50 m), together with the -70/-80

493   m and -85/-90 m terraces, are all affected by several NW–SE faults, located between Baía do Mar

494   da Barca and Baía da Cré (see Fig. 7). These faults extend inland, where they displace the subaerial

495   terraces up to 90 m in elevation, as with the "Aeroporto fault", or at Baía da Cré. The tectonic

496   structure in this sector suggests a compartmentalization of the volcanic edifice in grabens and

497   semi-grabens, where blocks with a relative downthrown movement experienced greater degrees

498   of coastal retreat, allowing also for the formation of depocenters where marine sedimentation

22

499   occurred. A similar situation can be observed along the deepest part of the shelf at the southern

500   sector (Fig. 9). Here, terrace geometry and distribution are somewhat controlled by several

501   tectonic lineaments (roughly oriented NNE–SSW) that may either correspond to faults, or to dikes

502   that served as limiting barriers to erosion and sedimentation. The NW-SE lineament offshore

503   Campo Grande, in the western shelf sector (Fig. 8), also limits the -70/-80 m terrace to the south

504   of this lineament. These features show that local vertical tectonics played an important role in the

505   development of submerged marine terraces, a role that needs further investigation. However,

506   these local effects do not influence the overall depth ranges of marine terraces.

507

508   *5.4 TERRACE FORMATION AND PRESERVATION*

509

510   As far as we know, Santa Maria is the only reefless volcanic island that has submerged terraces

511   mapped with high detail. Most of the studies about terraces on volcanic islands are from reefal

512   settings and are almost exclusively off Hawaii (e.g., Campbell, 1986; Faichney et al., 2010).

513   Terraces in reef settings are mostly constructional in origin and hence they are of little utility for a

514   comparison with our study. Nevertheless, some inferences can be made based on modelling of

515   erosional terraces (Trenhaile, 2002; 2014) and the geological record of raised and submerged

516   terraces in other settings.

517   Raised terraces in Santa Maria are moderately well preserved despite their relatively old age

518   (3.436-1.065 Ma). However, terraces developed on islands and on relatively narrow landmasses

519   tend to be better preserved because the length of the streams is limited and so is the erosion of

520   the landscape (Anderson et al., 1999). Two contrasting hypotheses regarding the

521   formation/preservation of the terraces have been found in the literature. According to Pedoja et

522   al. (2014) coastal staircase sequences are present mainly in areas where apparent uplift rates are

        23

very low to moderate, because sea level must remain stationary long enough to allow for the formation of these features. Their compilation of subaerial terraces in hotspot settings shows that these occur on islands with average uplift rates of 0.01 mm/yr. However, modelling by Trenhaile (2002; 2014) suggest that only rapid uplift rates are able to preserve terraces, otherwise these are removed by erosion and cliff retreat during periods following high, interglacial sea level. Trenhaile (2014) considers 0.02 mm/yr as slow uplift rates and 0.1 mm/yr as fast. Our data agree with the model presented by Trenhaile (2014). In fact, estimated uplift rates for Santa Maria (0.042/0.059 mm/yr) fall between those two values of Trenhaile (2014), which might explain why the terraces are relatively well preserved.

As for submerged terraces, modelling by Trenhaile (2014) suggests that very narrow terraces form on uplifting coasts (figure 6 of Trenhaile, 2014). According to this author, this is because submerged terraces are preferentially formed during lowstands and are subsequently modified (or even eliminated) during periods of rising and falling sea as they are uplifted. Our observations support, however, the preservation of different orders of submerged terraces on the shelf of Santa Maria. Not surprisingly, the average width (Table 3ESM) of the submerged terraces of Santa Maria is smaller (normally < 200 m if we exclude the northern sector) than the width of the subaerial terraces (300-500 m). A likely explanation lies in the fact, already discussed above, that submerged terraces here bear the strong imprint of sea-level changes with much higher amplitude and lower frequency in the late Quaternary than the raised terraces formed in early-middle Quaternary (Fig. 15). According to Trenhaile (2014) the scale of sea-level oscillations has an important effect on shelf width, which increases with increasing eustatic amplitude on uplifting landmasses. The fact that submarine terraces are systematically eroded by passing sea level as the shelf widens, also contributes to a final morphology in which clearly preserved terraces are apparently not as wide as subaerial terraces.

24

547

6. CONCLUSIONS

In this study we analyzed for the first time the possible correlation between the formation of the subaerial and submerged terraces with known sea-level changes, on a reefless volcanic island setting. Our approach, including the integration of newly available high-resolution marine geophysical data with detailed onshore field studies, allowed us to:

 - recognize five sets of submerged marine terraces located at different depths.

- better estimate the uplift rates for Santa Maria island, using two dated raised, subaerial paleoshorelines and a composite sea level curve. Those rates were used to determine the possible age interval of formation of subaerial and submerged marine terraces, ranging from 3.436 Ma to 12.1 ka BP, being formed and later modified by more than one passage of sea level.

- analyze the controlling factor of the submerged marine terraces distribution. On low gradient, and consequently wider shelves, terraces are more easily carved/preserved. Conversely, steeper shelf gradients facilitate the erosion of upper and older terraces by younger and deeper terraces in uplifting areas.

- better constraint the faulting activity at least to the 0.693–2.7 Ma period, based on the offset experienced by subaerial and submerged terraces. Activity could have been more prolonged in time, but degradation of the subaerial terraces and lack of clear evidence on the submerged ones does not allow us to extend further that period.

- propose an original and consistent reconstruction for the marine terraces formation at Santa Maria, notwithstanding the complex interplay between glacio-eustatic oscillations, marine erosion, and island uplift.

569

25

580

581 *REFERENCES*

582

583 Anderson R.S., Densmore A.L., Ellis, M.A., 1999. The generation and degradation of marine

584 terraces. Basin Research 11: 7–19. doi: 10.1046/j.1365-2117.1999.00085.x

585

586 Andrade, C., Trigo, R.M., Freitas, M.C., Gallego, M.C., Borges, P., Ramos, A.M., (2008). Comparing

587 historic records of storm frequency and the North Atlantic Oscillation (NAO) chronology for the

588 Azores region. Holocene 18(5), 745–754. doi:10.1177/0959683608091794.

589

590 Antonioli, F., Kershaw, S., Rust, D., Verrubbi, V., 2003. Holocene sea-level change in Sicily and its

591 implications for tectonic models: new data from the Taormina area, northeast Sicily. Mar. Geol.

592 3293, 1–19.

593

26

594 Ávila, S.P., Madeira, P., Da Silva, C.M., Cachão, M., Landau, B., Quartau, R. and Martins, A.M.,

595 2008. Local disappearance of bivalves in the Azores during the last glaciation. Journal of

596 Quaternary Science 23, no.8, p. 777-785.

597

598 Ávila, S.P., Melo, C., Silva, L., Ramalho, R.S., Quartau, R., Hipólito, A., Cordeiro, R., Rebelo, A.C.,

599 Madeira, P., Rovere, A., Hearty, P.J., 2015c. A review of the MIS 5e highstand deposits from Santa

600 Maria Island (Azores, NE Atlantic): Palaeobiodiversity, palaeo- ecology and palaeobiogeography.

601 Quaternary Science Reviews. 114, p. 126–148. doi:10.1016/j.quascirev .2015.02.012.

602

603 Bintanja, R., van de Wal, R.S., 2008. North American ice-sheet dynamics and the onset of 100,000-

604 year glacial cycles. Nature 454(7206):869-72. doi: 10.1038/nature07158.

605

606 Blanchon P, Jones B., 1995. Marine-Planation Terraces on the Shelf around Grand Cayman - a

607 Result of Stepped Holocene Sea-Level Rise. J. Coast. Res. 11(1), 1-33. PubMed PMID: WOS:

608 A1995QG34200001.

609

610 Callapez, P., Soares, A.F., 2000. Late Quaternary marine mollusks from Santa Maria (Azores);

611 paleoecologic and paleobiogeographic considerations. Ciências Terra (UNL) 14, 313-322.

612

613 Campbell, J.F., 1986. Subsidence rates for the Southeastern Hawaiian Islands determined from

614 submerged terraces. Geo-Marine Letters. 6(3), 139-46.

615

616 Caputo, R., 2007. Sea-level curves: Perplexities of an end-user in morphotectonic applications.

617 Global and Planetary Change. 57(3-4), 417-23.

618

619 Casalbore, D., Falese, F., Martorelli, E., Romagnoli, C., Chiocci, F.L., 2017a. Submarine depositional

620 terraces in the Tyrrhenian Sea as a proxy for paleo-sea level reconstruction: Problems and

621 perspective. Quat. Int. 439, 169–180. 10.1016/j.quaint. 2016.07.051.

622

623 Cas, R., Wright, J., 1987. Volcanic Successions. Modern and Ancient: A Geological Approach to

624 Processes, Products and Successions: London, Chapman & Hall 528, p. doi: 10 .1007 /978 -94 -009

625 -3167 -1.

626

627 Coulbourn, W.T., Campbell, J.F., Moberly, R., 1974. Hawaiian submarine terraces, canyons and

628 quaternary history evaluated by seismic-reflection profiling. Mar Geol. 17, 215-34.

629

630 De Boer, B., Van De Wal, R.S.W., Bintanja, R., Lourens, L.J., Tuenter, E., 2010. Cenozoic global ice-

631 volume and temperature simulations with 1-D ice-sheet models forced by benthic 18O records.

632 Annals of Glaciology. 51(55), 23-33.

633

634 De Guidi, G., Monaco, C., 2009. Late Holocene vertical deformation along the coast of Pantelleria

635 Island (Sicily Channel, Italy). Quaternary International, 206, 158-165.

636

637 Faichney, I.D.E., Webster, J.M., Clague, D.A., Paduan, J.B., Fullagar, P.D., 2010. Unraveling the

638 tilting history of the submerged reefs surrounding Oahu and the Maui-Nui Complex, Hawaii.

639 Geochem Geophys Geosyst. 11(7), Q07002.

640

28

641 Ferranti, L., Antonioli, F., Mauz, B., Amorosi, A., Dai, Pra G., Mastronuzzi, G., Monaco, C., Orrù, P.,

642 Pappalardo, M., Radtke, U., Renda, P., Romano, P., Sansò, P., Verrubbi, V., 2006. Markers of the

643 last interglacial sea-level high stand along the coast of Italy: tectonic implications. Quat. Int. 145–

644 146, 30–54.

645

646 Firth, C., Stewart, I., McGuire, W.J., Kershaw, S., Vita-Finzi, C., 1996. Coastal elevation changes in

647 eastern Sicily: implications for volcano instability at Mount Etna. In:McGuire, W.J., Jones, A.P.,

648 Neuberg, J. (Eds.), Volcano Instability on the Earth and Other Planets. Geol. Soc. London Spec.

649 Publ. 80, pp. 57–74.

650

651 Gente, P., Dyment, J., Maia, M., and Goslin, J., 2003. Interaction between the Mid-Atlantic Ridge

652 and the Azores hotspot during the last 85 Myr: Emplacement and rifting of the hot spot-derived

653 plateaus. Geochemistry, Geophysics, Geosystems. 4, no. 10, 8514.

654

655 Instituto Hidrográfico (Ed), 2000. Arquipélago dos Açores, 2nd edn, Roteiro da Costa de Portugal

656 Instituto Hidrográfico, Lisboa.

657

658 Hipólito, A., Madeira, J., Carmo, R., and Gaspar, J.L., 2013. Neotectonics of Graciosa Island

659 (Azores): a contribution to seismic hazard assessment of a volcanic area in a complex geodynamic

660 setting. Annals of Geophysics. 56, no. 6, S0677.

661

662 Lourenço, N., Miranda, J.M., Luís, J.F., Ribeiro, A., Victor, L. M., Madeira, J., and Needham, H.,

663 1998. Morpho-tectonic analysis of the Azores Volcanic Plateau from a new bathymetric

664 compilation of the area. Marine Geophysical Researches. 20, no. 3, p. 141–156.

29

665

666 Lucchi, F., Tranne, C.A., Calanchi, N., Rossi, P.L., 2007. Late Quaternary deformation history of the

667 volcanic edifice of Panarea (Aeolian Arc). Bull. Volcanol. 69, 239–257.

668

669 Lucchi, F. 2009. Late-Quaternary marine terrace deposits as tools for wide-scale correlation of

670 unconformity-bounded units in the volcanic Aeolian archipelago (southern Italy). Sedimentary

671 Geology. 216, 158–178.

672

673 Madeira, J., Brum da Silveira, A., Hipólito, A., & Carmo, R. (2015). Chapter 3 Active tectonics in the

674 central and eastern Azores islands along the Eurasia-Nubia boundary: a review. Geological Society,

675 London, Memoirs. 44(1), 15–32. https://doi.org/10.1144/M44.3.

676

677 Marques, F.O., Catalão, J.C., DeMets, C., Costa, A.C.G., and Hildenbrand, A., 2013. GPS and

678 tectonic evidence for a diffuse plate boundary at the Azores Triple Junction. Earth and Planetary

679 Science Letters. 381, p. 177–187.

680

681 Mauz, B., Vacchi, M., Green, A., Hoffmann, G., Cooper, A., 2015. Beachrock: A tool for

682 reconstructing relative sea level in the far-field. Mar Geol. 362(0), 1-16. doi:

683 dx.doi.org/10.1016/j.margeo.2015.01.009.

684

685 Meireles, R.P., Quartau, R., Ramalho, R.S., Rebelo, A.C., Madeira, J., Zanon, V., and Ávila, S.P.,

686 2013. Depositional processes on oceanic island shelves—Evidence from storm-generated Neogene

687 deposits from the mid-North Atlantic. Sedimentology. 60, no. 7, p. 1769–1785, doi: 10 .1111 /sed

688 .12055.

689

690   Miller, K., Kominz, M., Browning, J., Wright, J., Mountain, G., Katz, M., Sugarman, P., Cramer, B.,

691   Christie-Blick, N., and Pekar, S., 2005. The Phanerozoic record of global sea-level change. Science.

692   V. 310, no. 5752, p. 1293–1298, doi:10.1126/science.1116412.

693

694   Miranda, J.M., Luís, J.F., and Lourenço, N., 2018. The geophysical architecture of the Azores from

695   magnetic data, in Küppers, U., and Beier, C., eds., Volcanoes of the Azores. Active Volcanoes of the

696   World. Berlin, Springer Verlag. 89-100.

697

698   Passaro,S., Ferranti, L., and de Alteriis, G. 2011. The use of high-resolution elevation histograms for

699   mapping submerged terraces: Tests from the Eastern Tyrrhenian Sea and the Eastern Atlantic

700   Ocean. Quaternary International, 232 (1-2), 238-249.

701

702   Pirazzoli, P.A., Radtke, U., Hantoro, W.S., Jouannic, C., Hoang, C.T., Causse, C., et al. 1993. A one

703   million-year-long sequence of marine terraces on Sumba Island, Indonesia. Marine Geology.

704   109(3), 221-236.

705

706   Pedoja, K., Husson, L., Johnson, M.E., Melnick, D., Witt, C., Pochat, S., Nexer, M., Delcaillau, B.,

707   Pinegina, T., Poprawski, Y., Authemayou, C., Elliot, M., Regard, V., Garestier, F., 2014. Coastal

708   staircase sequences reflecting sea-level oscillations and tectonic uplift during the Quaternary and

709   Neogene. Earth-Sci. Rev. 132, 13-38.

710

711   Porębski, S., and Gradziński, R., 1990. Lava-fed Gilbert type delta in the Polonez Cove Formation

712   (Lower Oligocene), King George Island, West Antarctica, in Colella, A., and Prior, D., eds., Coarse

31

713   Grained Deltas. International Association of Sedimentologists Special Publication 10, p. 333–351,

714   doi: 10 .1002/9781444303858.ch19.

715

716   Quartau, R., Tempera, F., Mitchell, N.C., Pinheiro, L.M., Duarte, H., Brito, P.O., Bates, R., Monteiro,

717   J.H., 2012. Morphology of the Faial Island shelf (Azores): the interplay between volcanic, erosional,

718   depositional, tectonic and mass-wasting processes. Geochemistry, Geophysics, Geosystems. 13,

719   Q04012. DOI: 10.1029/ 2011GC003987.

720

721   Quartau, R., Mitchell, N.C., 2013. Comment on "Reconstructing the architectural evolution of

722   volcanic islands from combined K/Ar, morphologic, tectonic, and magnetic data: The Faial Island

723   example (Azores)" by Hildenbrand et al. (2012). [J. Volcanol. Geotherm. Res. 241-242 (2012) 39-

724   48]. J Volcanol Geotherm Res. 255, 124-6.

725

726   Quartau, R., Hipólito, A., Romagnoli, C., Casalbore, D., Madeira, J., Tempera, F., Roque, C. and

727   Chiocci, F.L., 2014. The morphology of insular shelves as a key for understanding the geological

728   evolution of volcanic islands: Insights from Terceira Island (Azores), Geochemistry, Geophysics,

729   Geosystems. 15, 1801–1826.

730

731   Quartau R., Madeira J., Mitchell N.C., Tempera F., Silva P.F., Brandao F., 2015. The insular shelves

732   of the Faial-Pico Ridge (Azores archipelago): a morphological record of its evolution.

733   Geochemistry, Geophysics, Geosystems 16, 1401-1420.

734

735   Ramalho, R.S., 2011, Building the Cape Verde Islands (1st ed.): Berlin, Springer, 207 p., doi: 10

736   .1007 /978 -3 -642-19103 -9 .

32

737

738 Ramalho, R.S., Helffrich, G., Schmidt, D.N., and Vance, D., 2010a. Tracers of uplift and subsidence

739 in the Cape Verde Archipelago: Journal of the Geological Society of London 167, no. 3, p. 519–538,

740 doi: 10 .1144 /0016-76492009 -056.

741

742 Ramalho, R.S., Helffrich, G., Cosca, M., Vance, D., Hoffmann, D., and Schmidt, D.N., 2010b. Episodic

743 swell growth inferred from variable uplift of the Cape Verde hotspot islands: Nature Geoscience 3,

744 no. 11, p. 774–777, doi: 10 .1038 /ngeo982.

745

746 Ramalho, R.S., Helffrich, G., Cosca, M., Vance, D., Hoffmann, D., and Schmidt, D.N., 2010c. Vertical

747 movements of ocean island volcanoes: Insights from a stationary plate environment. Marine

748 Geology 275, p. 84–95, doi: 10 .1016 /j .margeo .2010 .04 .009.

749

750 Ramalho, R.S., Quartau, R., Trenhaile, A.S., Mitchell, N.C., Woodroffe, C.D. and Ávila, S.P., 2013.

751 Coastal evolution on volcanic oceanic islands: A complex interplay between volcanism, erosion,

752 sedimentation, sea-level change and biogenic production. Earth-Science Reviews 127, p. 140-170.

753

754 Ramalho, R.S., Helffrich, G., Madeira, J., Cosca, M., Thomas, C., Quartau, R., Hipólito, A., Rovere,

755 A., Hearty, P., and Ávila, S.P. 2017. Emergence and evolution of Santa Maria Island (Azores) – The

756 conundrum of uplifted islands revisited. Geological Society America Bulletin 129, 2017 DOI:

757 10.1130/B31538.1.

758

759 Rusu, L., Guedes Soares, C., 2012. Wave energy assessments in the Azores islands. Renewable

760 Energy 45, 183-96.

761

762 Schwartz D.M., Soule S.A., Wanless V.D. and Jones M.R. 2018. Identification of Erosional Terraces

763 on Seamounts: Implications for Interisland Connectivity and Subsidence in the Galápagos

764 Archipelago. Front. Earth Sci. 6:88. doi: 10.3389/feart.2018.00088.

765

766 Sibrant, A.L.R., Hildenbrand, A., Marques, F.O., and Costa, A.C.G., 2015a. Volcano-tectonic

767 evolution of the Santa Maria Island (Azores): Implications for paleostress evolution at the western

768 Eurasia–Nubia plate boundary. Journal of Volcanology and Geothermal Research 291, p. 49–62.

769

770 Serralheiro, A., 2003. A geologia da ilha de Santa Maria, Açores. Açoreana 10, no. 1, p. 141–192.

771

772 Serralheiro, A., Alves, C.A.M., Forjaz, V.H., and Rodrigues,B., 1987. Carta Vulcanológica dos Açores.

773 Ilha de Santa Maria na escala 1/15 000 (folhas 1 e 2), Serviço Regional de Protecção Civil dos

774 Açores, Universidade dos Açores and Centro de Vulcanologia.

775

776 Trenhaile, A.S., 2002. Modeling the development of marine terraces on tectonically mobile rock

777 coasts. Mar Geol. 185, 341-61.

778

779 Trenhaile, A.S., 2014. Modelling the effect of Pliocene–Quaternary changes in sea level on stable

780 and tectonically active land masses. Earth Surf Proc Land. 39, 1221-35. doi: 10.1002/esp.3574.

781

782 Trenhaile, A.S., 2015. Coastal notches: Their morphology, formation, and function. Earth-Science

783 Reviews. 150, 285-304. doi: dx.doi.org/10.1016/j.earscirev.2015.08.003.

784

34

785   Zazo, C., Goy, J. L., Hillaire-Marcel, C., Gillot, P. Y., Soler, V., González, J. Á., Ghaleb, B. 2002. Raised

786   marine sequences of Lanzarote and Fuerteventura revisited - A reappraisal of relative sea-level

787   changes and vertical movements in the eastern Canary Islands during the Quaternary. Quaternary

788   Science Reviews 21(18–19), 2019–2046. doi: 10.1016/S0277-3791(02)00009-4.

789

790   Zazo, C., Goy, J.L., Dabrio, C.J., Soler, V., Hillaire-Marcel, C., Ghaleb, B., et al. 2007. Quaternary

791   marine terraces on Sal Island (Cape Verde archipelago). Quaternary Science Reviews. 26(7-8), 876-

792   93.

793

794   Zbyszewski, G., Ferreira, O.V., 1960. Carta geológica de Portugal, Ilha de Santa Maria (Açores),

795   scale 1:50 000: Serviços Geológicos de Portugal.

796

797   FIGURE CAPTIONS

798

799   **Fig. 1.** Map illustrating the geodynamic setting of the islands (western, central and eastern groups)

800   in the Azores Archipelago (islands in grey, Santa Maria Island in white) and how they straddle the

801   triple junction between the North American (NA), Eurasian (EU) and Nubian (NU) lithospheric

802   plates. MAR: Mid-Atlantic Ridge; PAR: Princess Alice Rift; EAFZ: Eastern Azores Fracture Zone; TR:

803   Terceira Rift; GF: Gloria Fault. The top-right inset shows the geographical setting of the Azores

804   Archipelago within the Northern Atlantic Ocean. Grey shading represents the deformation zone of

805   Terceira rift and of the inactive Princess Alice Rift. The bathymetry is derived from the EMODNET

806   web portal (http://portal.emodnet-bathymetry.eu), tectonic structures adapted from Miranda et

807   al. (2018).

808

35

809 **Fig. 2. (a)** Geological map of Santa Maria Island, and **(b)** WNW–ESE oriented cross-section.

810 Underlying digital elevation model (DEM) is generated from a 1/5000 scale digital altimetric

811 database. Note that the Porto Fm and Lower Pico Alto volcanic complex are not visible on the

812 map/section at this scale. SMA 18 and SMA 45: samples collected in the submarine lava flows

813 below the passage zone of Monte Gordo (see the text for further details). Modified after Ramalho

814 et al. (2017).

815

816 **Fig. 3.** Dataset used for this study, showing the seismic reflection profiles acquired during the

817 PLATMAR cruise. The multibeam survey covered the area shown by the seismic grid. Yellow dots

818 represent location of sound speed profiles collected during the multibeam survey. Bathymetry

819 shown in this figure (~200 m resolution) was derived from the EMODNET web portal

820 (http://portal.emodnet-bathymetry.eu); topography was constructed from a 1/5000 scale digital

821 altimetric database.

822

823 **Fig. 4.** Schematic representation showing the morphologic elements considered in this work.

824

825 **Fig. 5.** Shaded relief imagery of the subaerial part of Santa Maria Island (1:5000 scale, digital

826 altimetric database from Secretaria Regional do Turismo e Transportes of the Azores Government)

827 and surrounding shelf (derived from the multibeam bathymetry). Black lines represent the limits

828 of the Northern, Western, Southern and Eastern sectors described in the text. Colored solid and

829 dashed lines represent the location of the evident and inferred inner margins of subaerial marine

830 terraces (modified after Ramalho at al., 2017).

831

36

832   **Fig. 6.** Uplift trend of Santa Maria Island reconstructed on the base of a dated subaerial marine

833   terrace (the short blue line represent its current elevation) and a passage zone between subaerial

834   and submarine lava flows (the short black line represent its current elevation). In grey, the

835   composite sea-level curve of Bintanja and Van de Wal (2008) and De Boer et al., (2010). In black,

836   the same sea-level curve modified according to the adopted uplift rates (see text for details). The

837   black dots on the grey curve represent the highstands considered in our calculations.

838

839   **Fig. 7.** Map of the mapped terraces on the northern shelf sector. Colored lines offshore

840   correspond to the inner edge of each terrace, whilst the respective colored adjacent areas to their

841   extension. Colored lines onshore correspond to the inner edge of the raised terraces. The seismic

842   profile aa' is shown in fig. 11 and seismic profiles ee' and ff' are respectively shown in Figs. 1ESM

843   and 2ESM.

844

845   **Fig. 8.** Map of the mapped terraces on the western shelf sector. Legend is the same as in Fig. 7.

846   The seismic profile bb' is shown in Fig. 12.

847

848   **Fig. 9.** Map of the mapped terraces on the southern shelf sector. Legend is the same as in Fig. 7.

849   The seismic profile cc' is shown in Fig. 13.

850

851   **Fig. 10.** Map of the mapped terraces on the eastern shelf sector. Legend is the same as in Fig. 7.

852   The seismic profile dd' is shown in Fig. 14.

853

854   **Fig. 11.** Boomer seismic profile aa' showing the shelf morphology off the northern sector of Santa

855   Maria. Location of the seismic profile in Fig. 7.

37

856

Fig. 12. Boomer seismic profile bb' showing the shelf morphology off the western sector of Santa

858   Maria. Location of the seismic profile in Fig. 8.

859

860   **Fig. 13.** Boomer seismic profile cc' showing the shelf morphology off the southern shelf sector of

861   Santa Maria. Location of the seismic profile in Fig. 9.

862

863   **Fig. 14.** Boomer seismic profile dd' showing the shelf morphology off the eastern shelf sector of

864   Santa Maria. Location of the seismic profile in Fig. 10.

865

866   **Fig. 15.** Tentative correlation between the terraces and their possible timing of formation and

867   subsequent modification within eustatic sea-level oscillations. Colored horizontal bars represent

868   the admissible time interval during which each terrace might have been carved by marine erosion

869   according to sea-level fluctuations and island uplift. The vertical width of each bar represent the

870   elevation range of the terrace +/- 5 m (see the text for details). The dots/squares with different

871   colors represent sea-level highstands, lowstands or other stillstands within the respective time

872   frame for each terrace.

873

874   **Fig. 16.** Plot of the total area of the subaerial and submerged marine terraces for each shelf sector

875   against the effective time that sea level was at their vertical position. These graphs were based on

876   the measurement of the width of the terraces along several profiles drawn in Fig. 8ESM. Note that

877   the horizontal scale is different among shelf sectors.

878

879   ELECTRONIC SUPPLEMENTARY MATERIAL - CAPTION

880   **Fig. 1ESM.** Boomer seismic profile ee'. See location in Fig. 7 of the main text.

881

882   **Fig. 2 ESM.** Boomer seismic profile ff'. See location in Fig. 7 of the main text.

883

884   **Fig. 3 ESM.** Location of the interpreted seismic profiles of Figs. 4ESM, 5ESM, 6ESM and 7ESM.
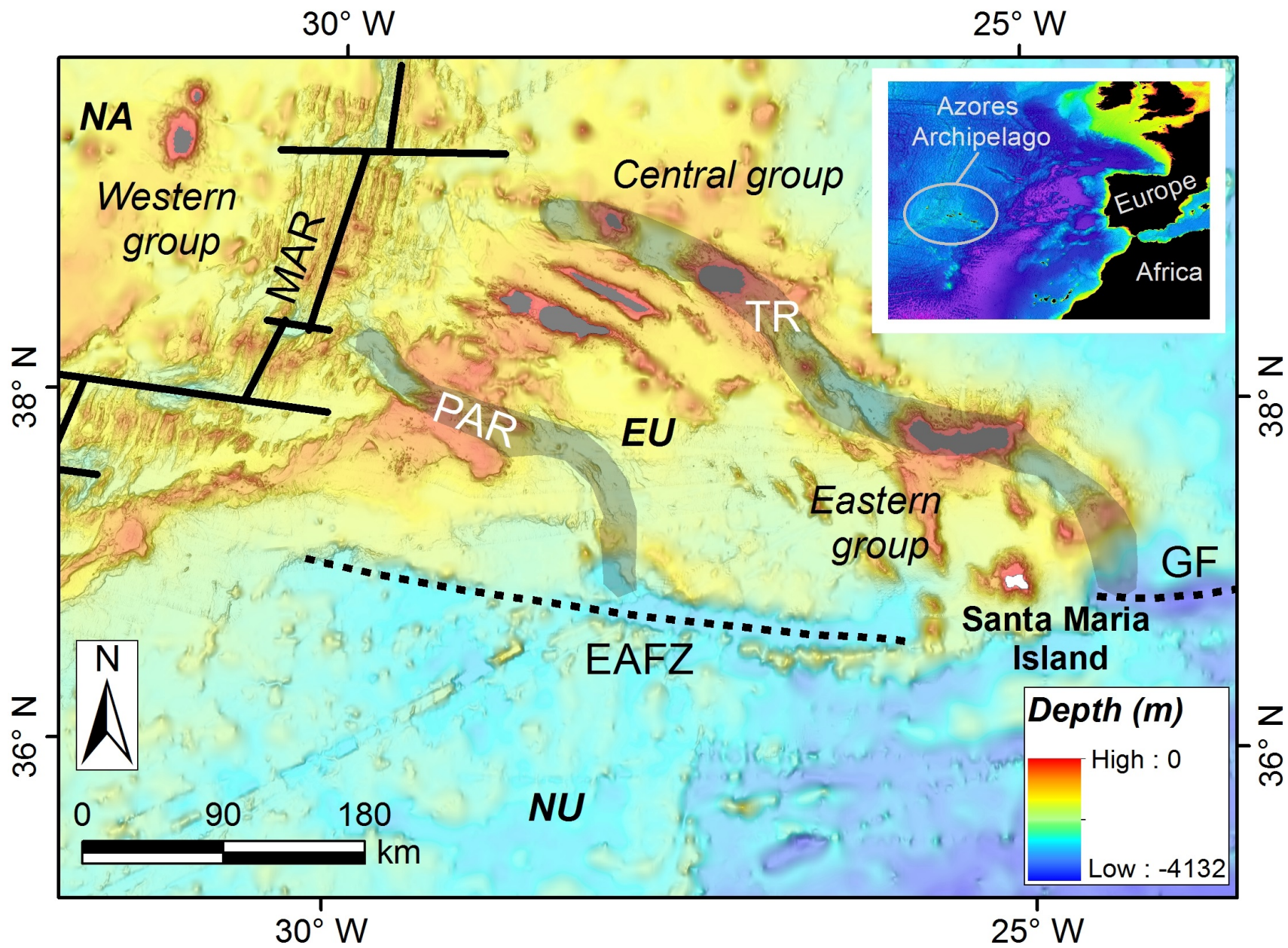
885

886   **Fig. 4 ESM.** Interpretation of the seismic profiles of the northern shelf sector showing the mapped
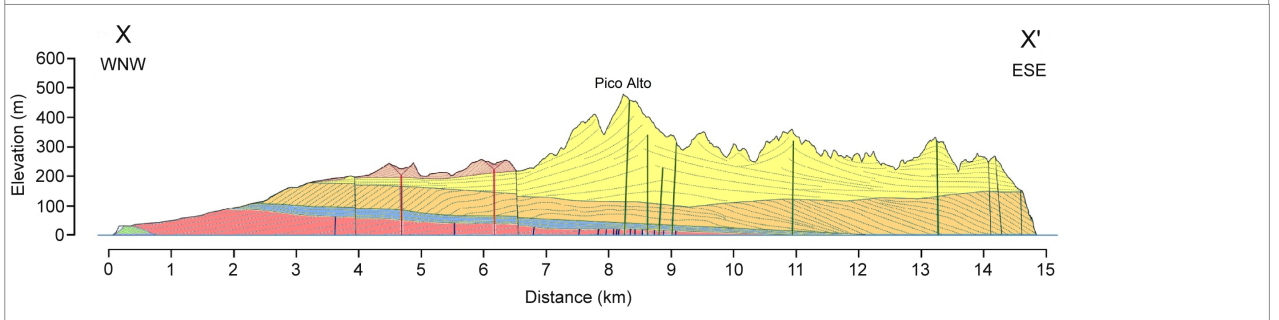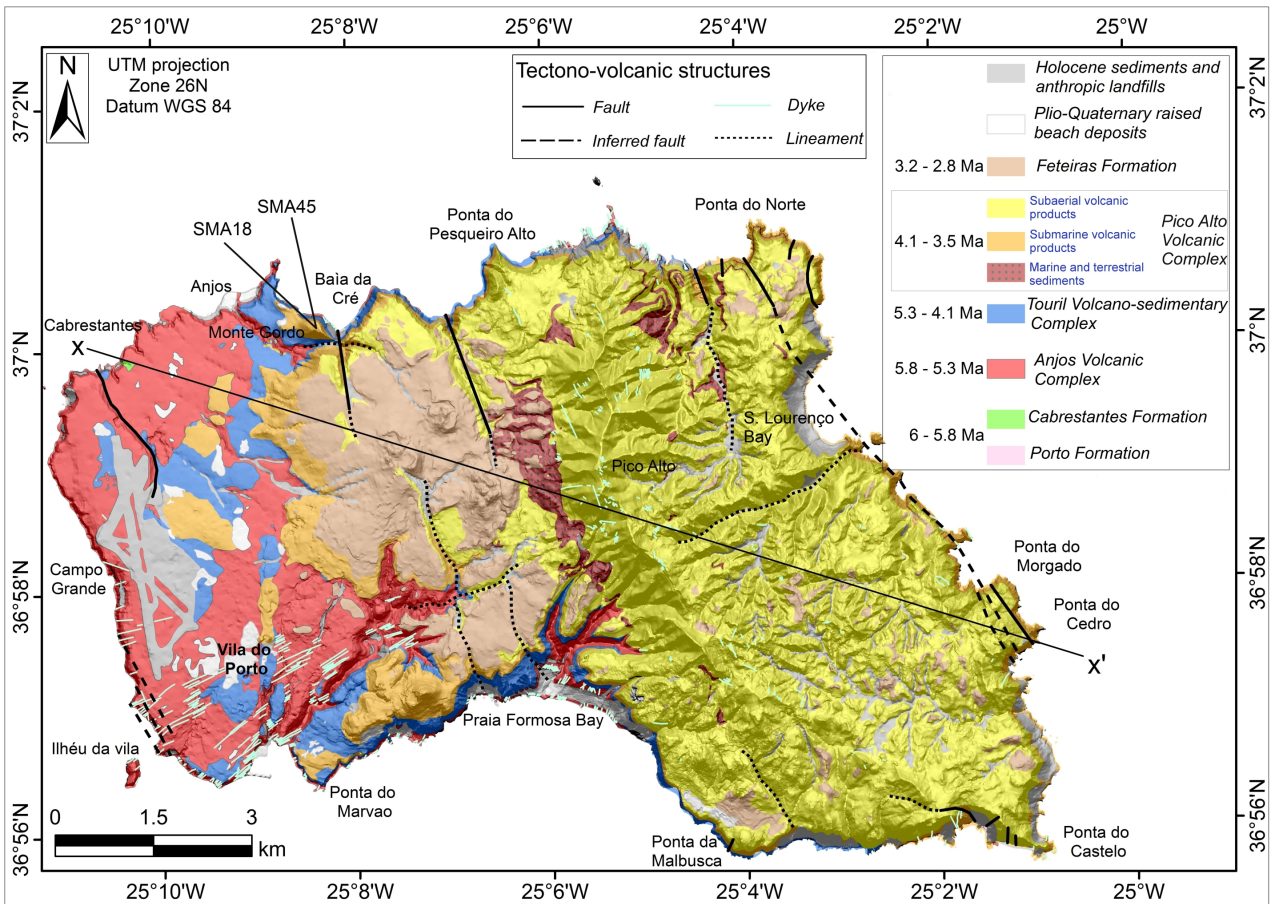
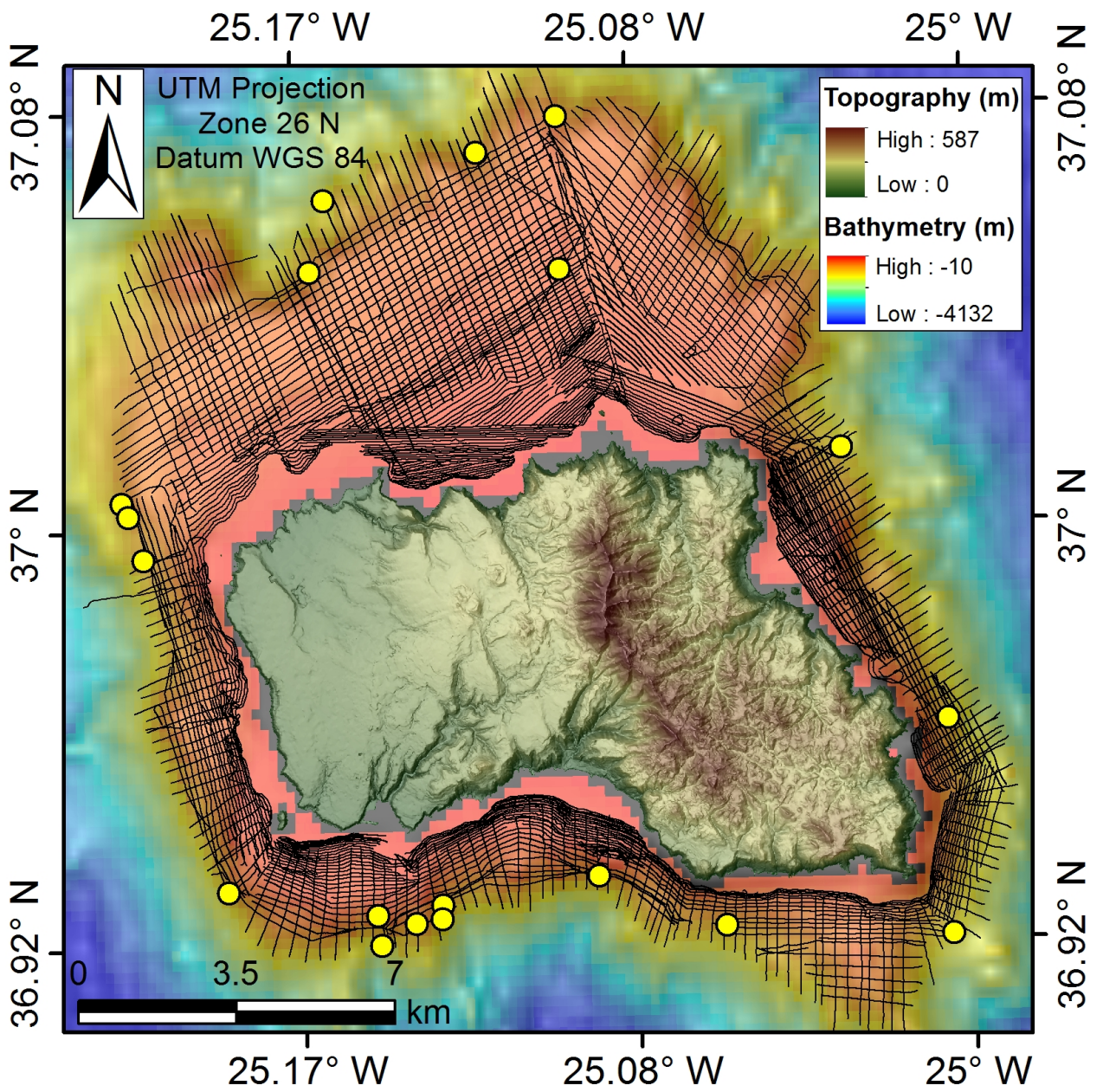887   terraces. Location of profiles shown in Fig. 3ESM.

888

889   **Fig. 5 ESM.** Interpretation of the seismic profiles of the western shelf sector showing the mapped

890   terraces. Location of profiles shown in Fig. 3ESM.

891

892   **Fig. 6 ESM.** Interpretation of the seismic profiles of the southern shelf sector showing the mapped

893   terraces. Location of profiles shown in Fig. 3ESM.

894

895   **Fig. 7 ESM.** Interpretation of the seismic profiles of the eastern shelf sector showing the mapped

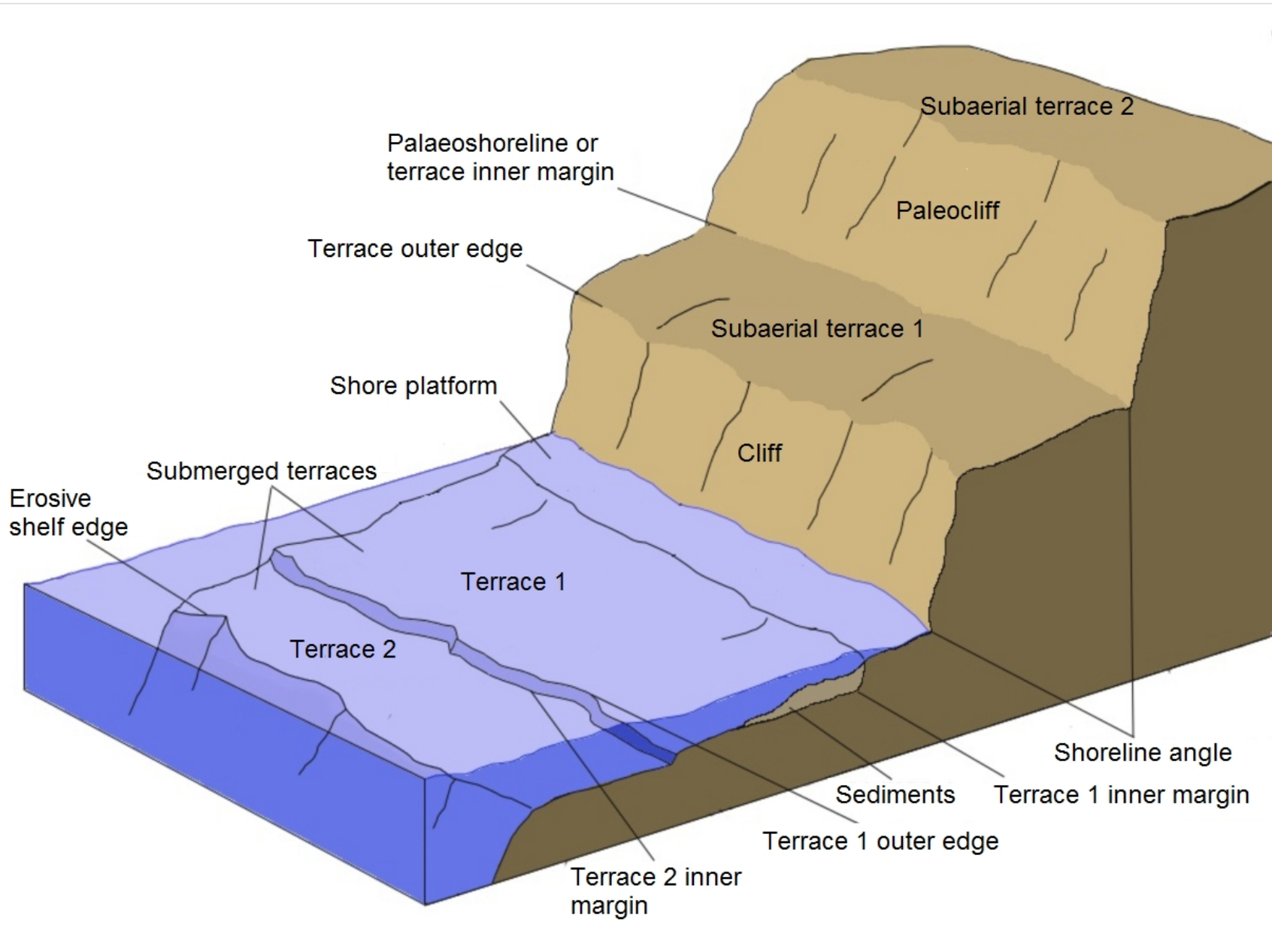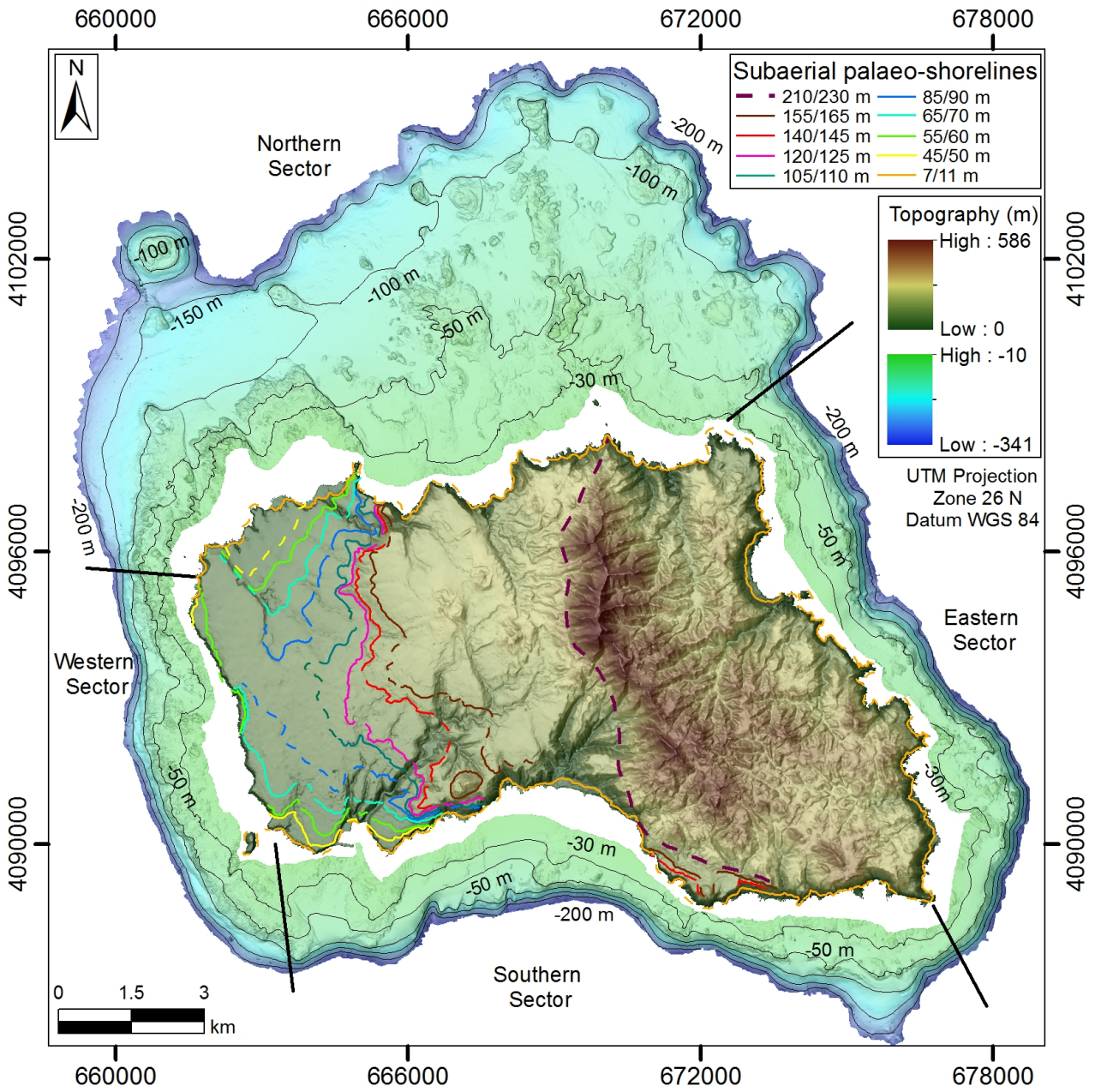896   terraces. Location of profiles shown in Fig. 3ESM.

897

898   **Fig. 8 ESM.** Location of the bathymetric profiles used to measure the width of the terraces in each

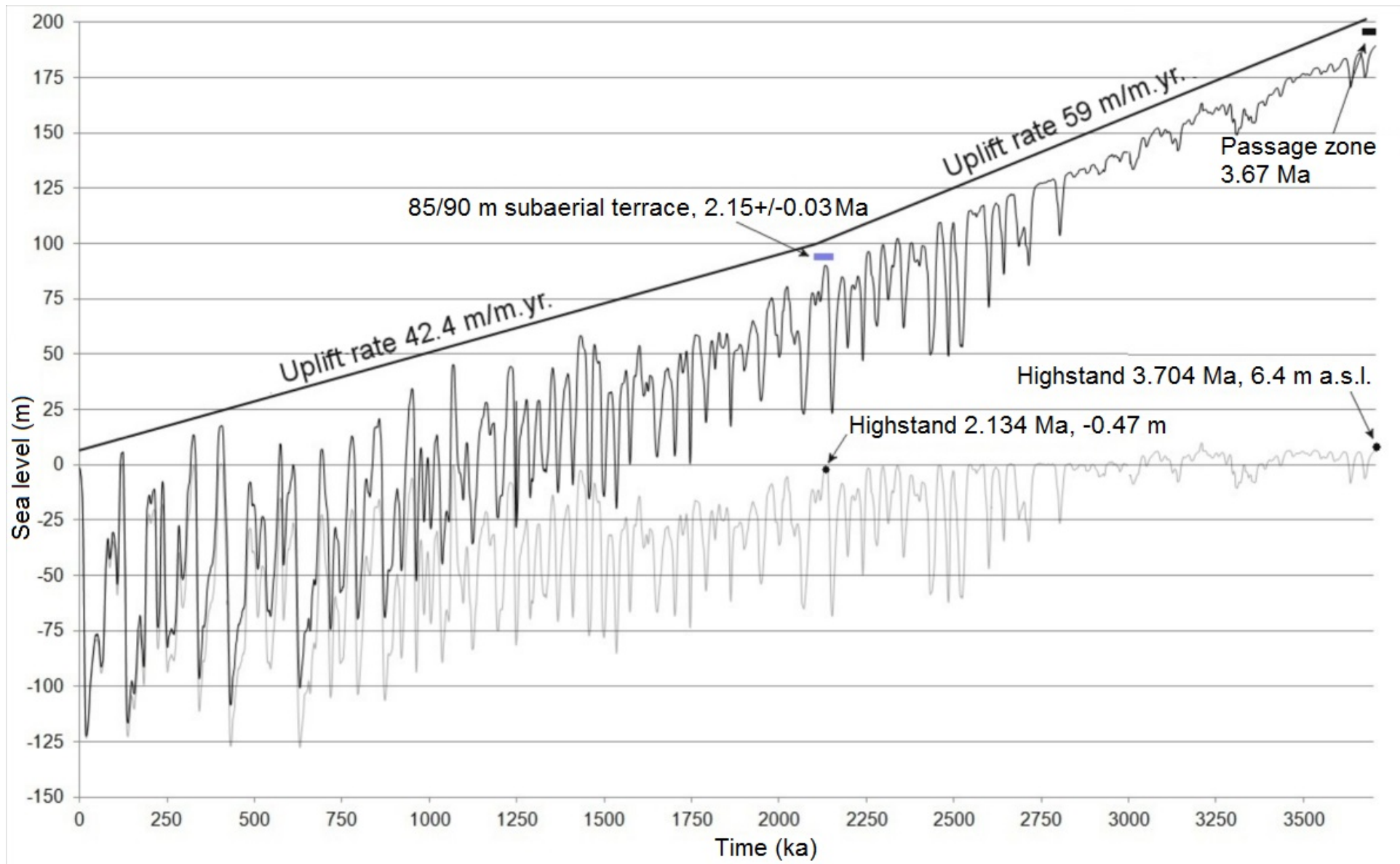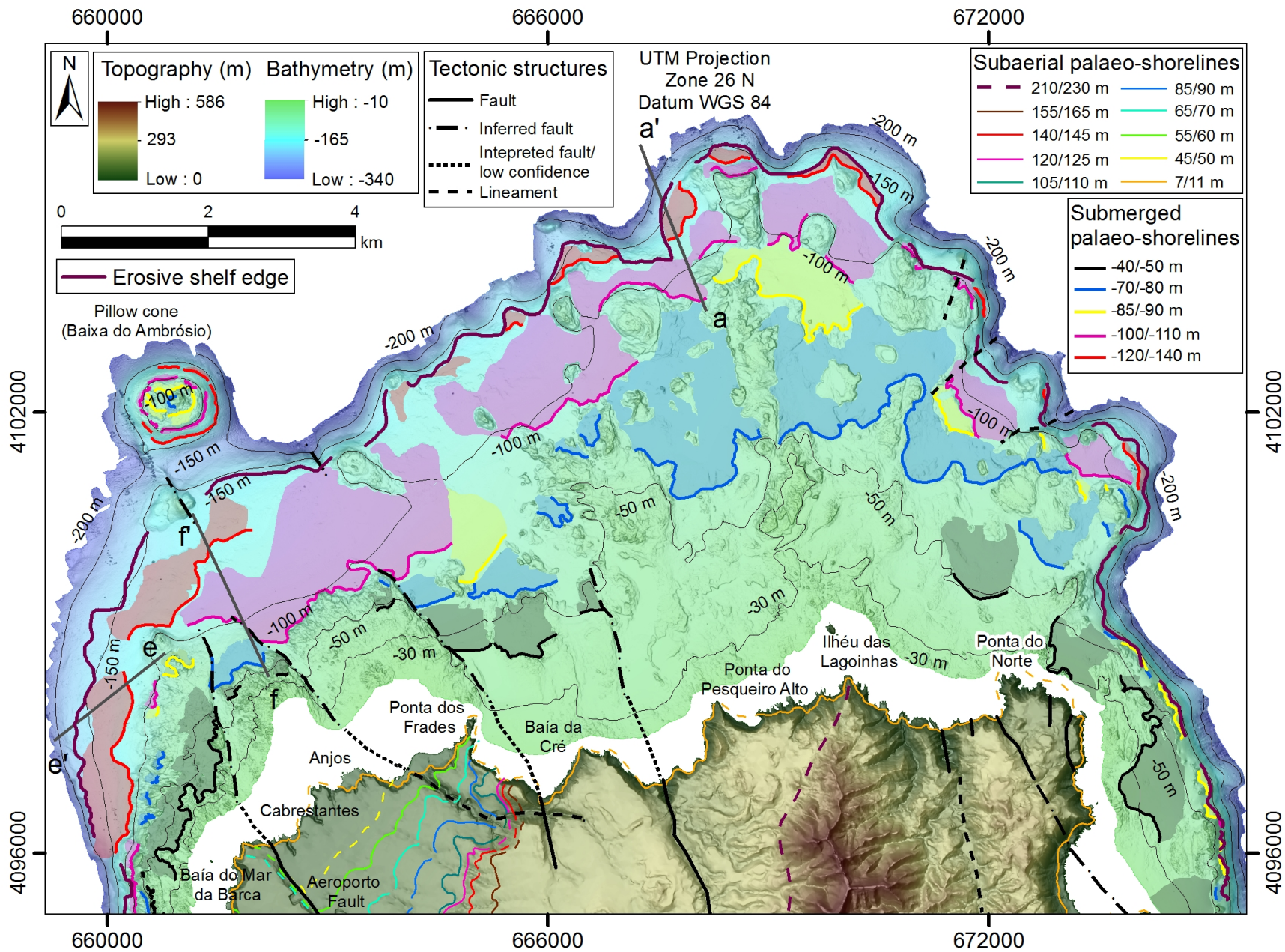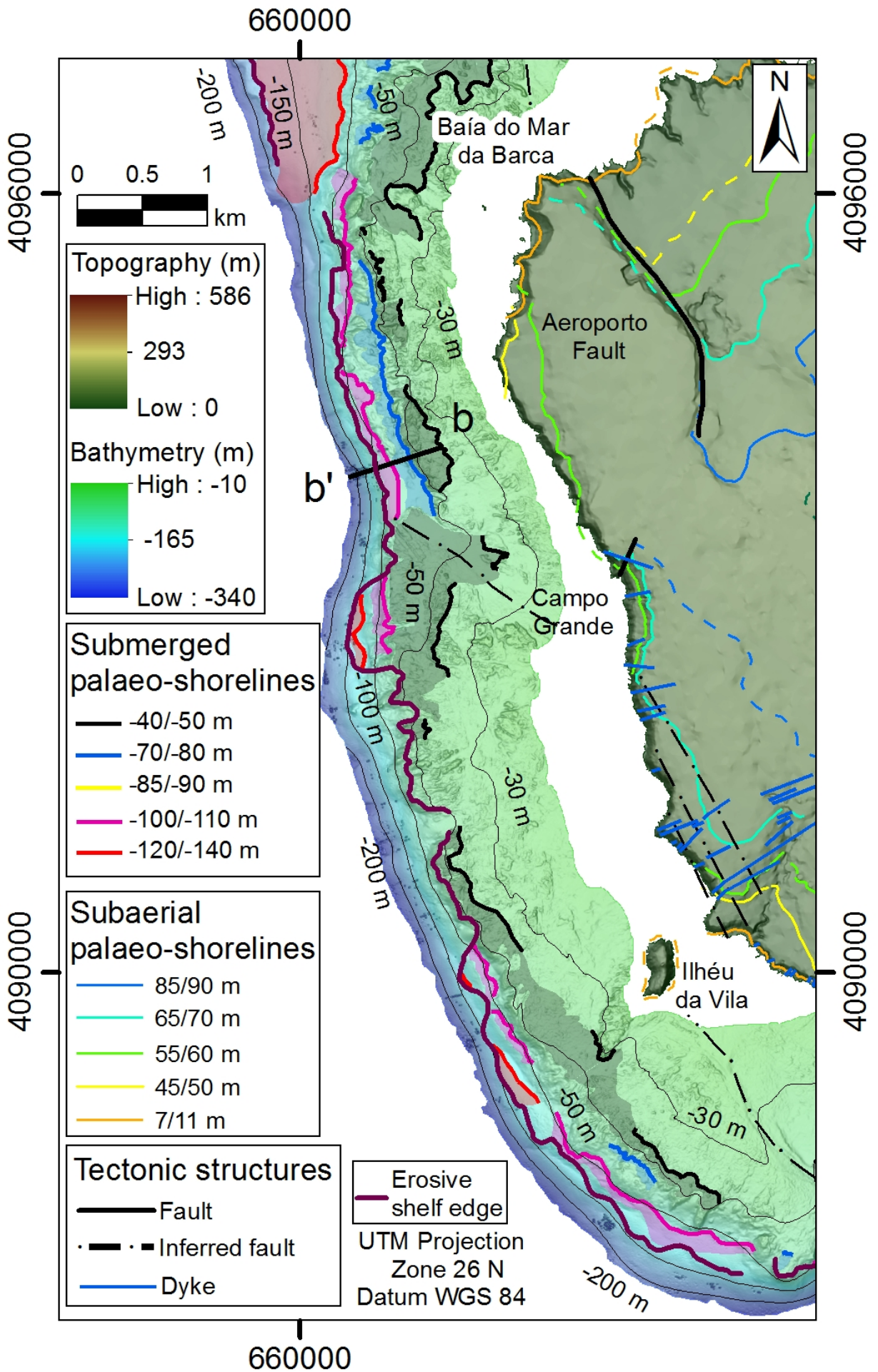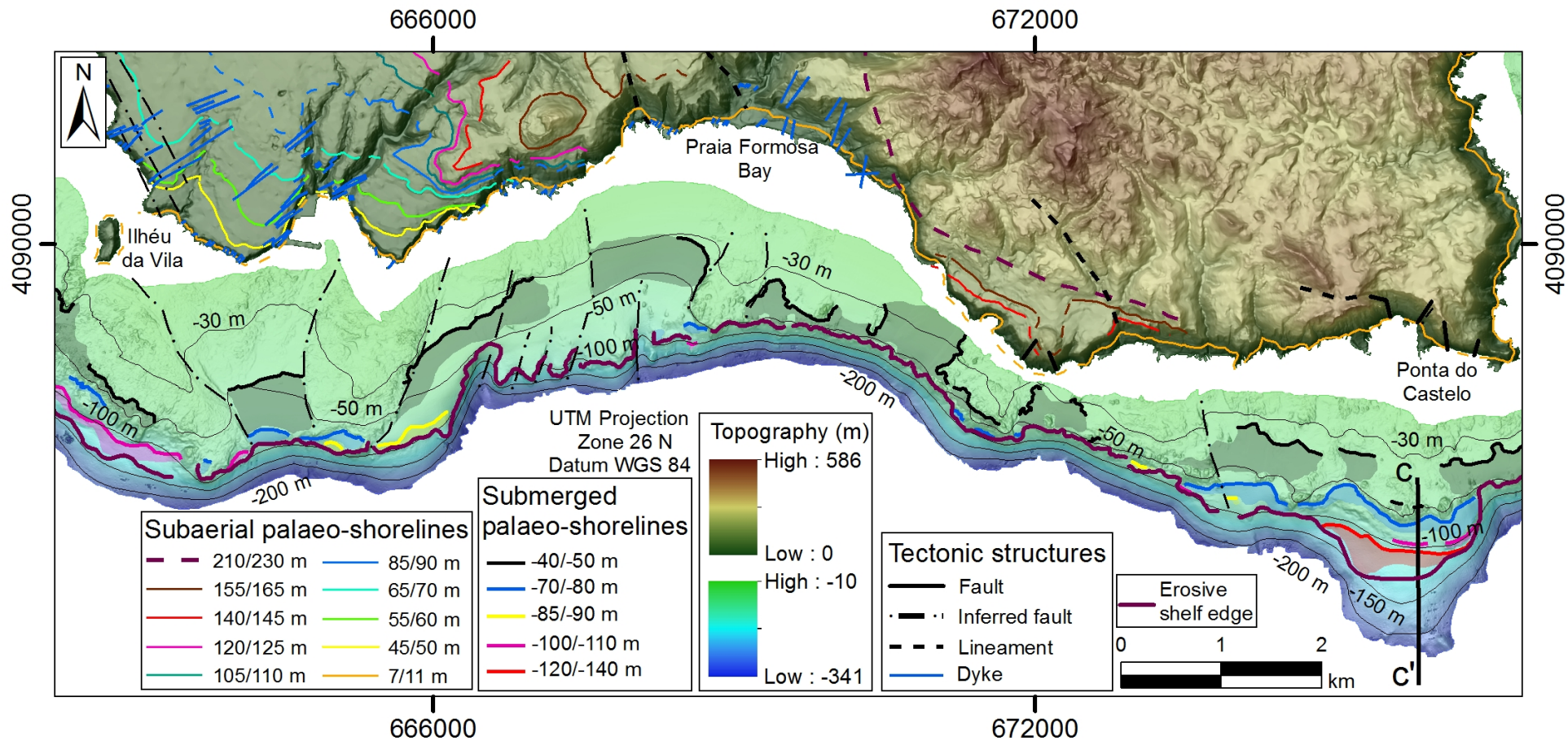899   shelf sector to provide the results of Fig. 16.

Map legend:

Tectono-volcanic structures
- Fault
- Inferred fault
- Dyke
- Lineament

- Holocene sediments and anthropic landfills
- Plio-Quaternary raised beach deposits
- 3.2 - 2.8 Ma — *Feteiras Formation*
- 4.1 - 3.5 Ma — Subaerial volcanic products / Submarine volcanic products / Marine and terrestrial sediments — *Pico Alto Volcanic Complex*
- 5.3 - 4.1 Ma — *Touril Volcano-sedimentary Complex*
- 5.8 - 5.3 Ma — *Anjos Volcanic Complex*
- 6 - 5.8 Ma — *Cabrestantes Formation* / *Porto Formation*

UTM projection Zone 26N Datum WGS 84

Map labels: SMA18, SMA45, Anjos, Cabrestantes, Monte Gordo, Baìa da Cré, Ponta do Pesqueiro Alto, Ponta do Norte, Pico Alto, S. Lourenço Bay, Campo Grande, Vila do Porto, Ilhéu da vila, Ponta do Marvao, Praia Formosa Bay, Ponta da Malbusca, Ponta do Morgado, Ponta do Cedro, Ponta do Castelo

Cross-section X – X' (WNW – ESE), Elevation (m) vs Distance (km), Pico Alto

Figure showing sea level (m) versus time (ka) with uplift curves. Labels include:
- Uplift rate 59 m/m.yr.
- Uplift rate 42.4 m/m.yr.
- 85/90 m subaerial terrace, 2.15+/-0.03 Ma
- Passage zone 3.67 Ma
- Highstand 3.704 Ma, 6.4 m a.s.l.
- Highstand 2.134 Ma, -0.47 m

Figure. Seismic profile showing submerged terraces. The legend "Submerged Terraces" indicates: -40/-50 m (black), -70/-80 m (blue), -100/-110 m (pink), -120/-140 m (red). Labels include "Terrace inner margin", "Sediments", and "Erosive shelf edge". Orientation N (left) to S (right). Depth axis in meters (0–150 m). Scale bar: 0 to 250 m.

WNW   ESE

Depth (m)

0

50

100

● Terrace inner margin

Submerged terraces

-40/-50 m ▬▬

-70/-80 m ▬▬

Sediments

Erosive shelf edge

0   250 m

Legend:

Subaerial Terraces
- 7/11 m (teal square)
- 45/50 m (yellow square)
- 55/60 m (light green square)
- 65/70 m (pale green square)
- 85/90 m (cyan square)
- 105/110 m (dark green square)
- 120/125 m (magenta square)
- 140/145 m (blue-grey square)
- 155/165 m (dark red square)

Submerged terraces
- -40/50 m (black circle)
- -70/-80 m (blue circle)
- -85/-90 m (orange circle)
- -100/-110 m (pink circle)
- -120/-140 m (red circle)

Uplift trend c. 59 m/Ma

Uplift trend c. 42 m/Ma

Sea level (m)
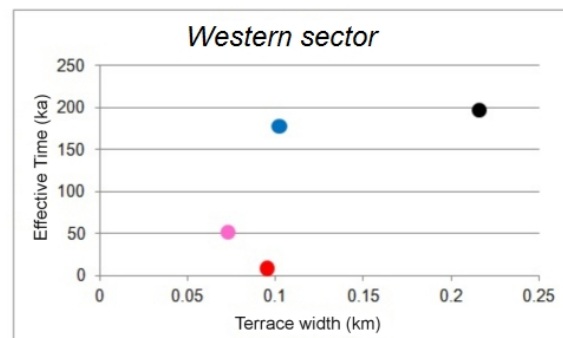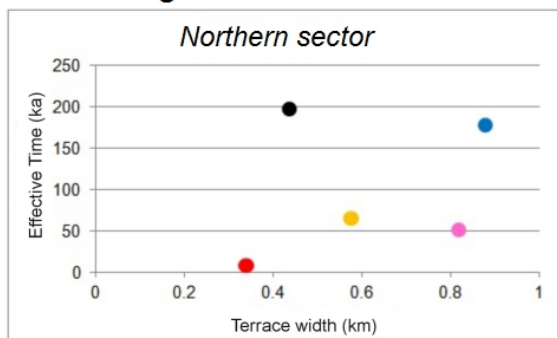
Time (ka)

Subaerial terraces
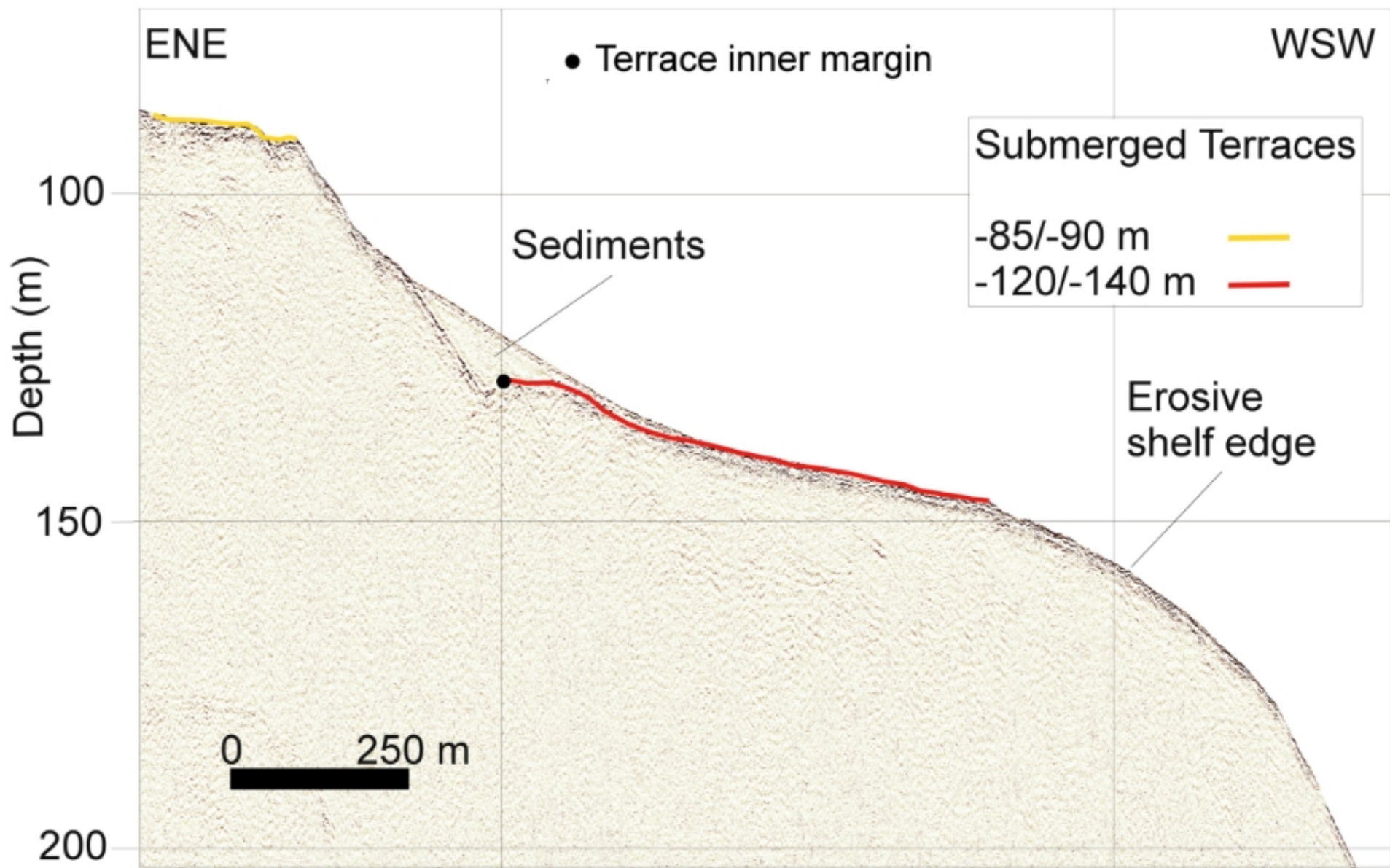
Legend

Subaerial terraces

45/50 m
55/60 m
65/70 m
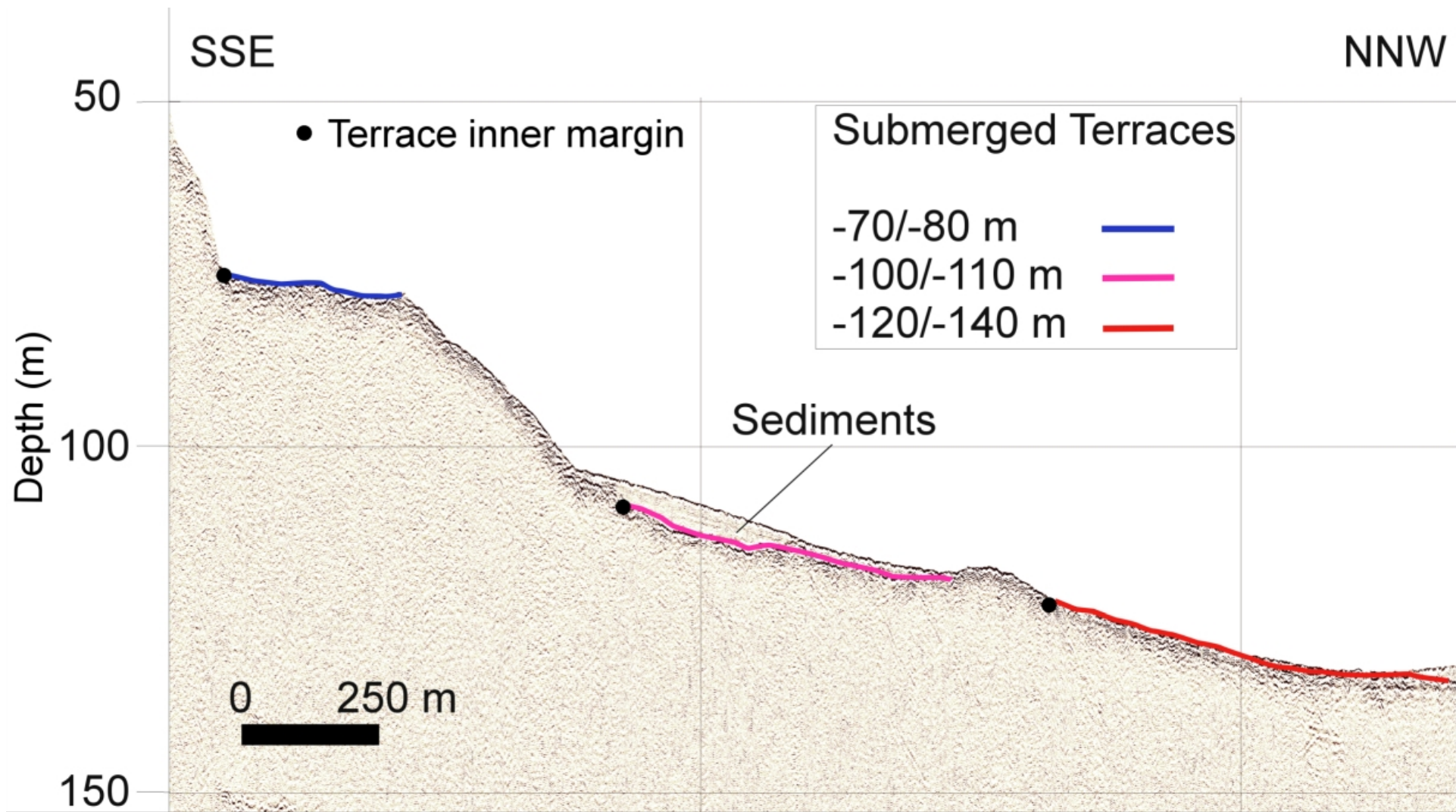85/90 m
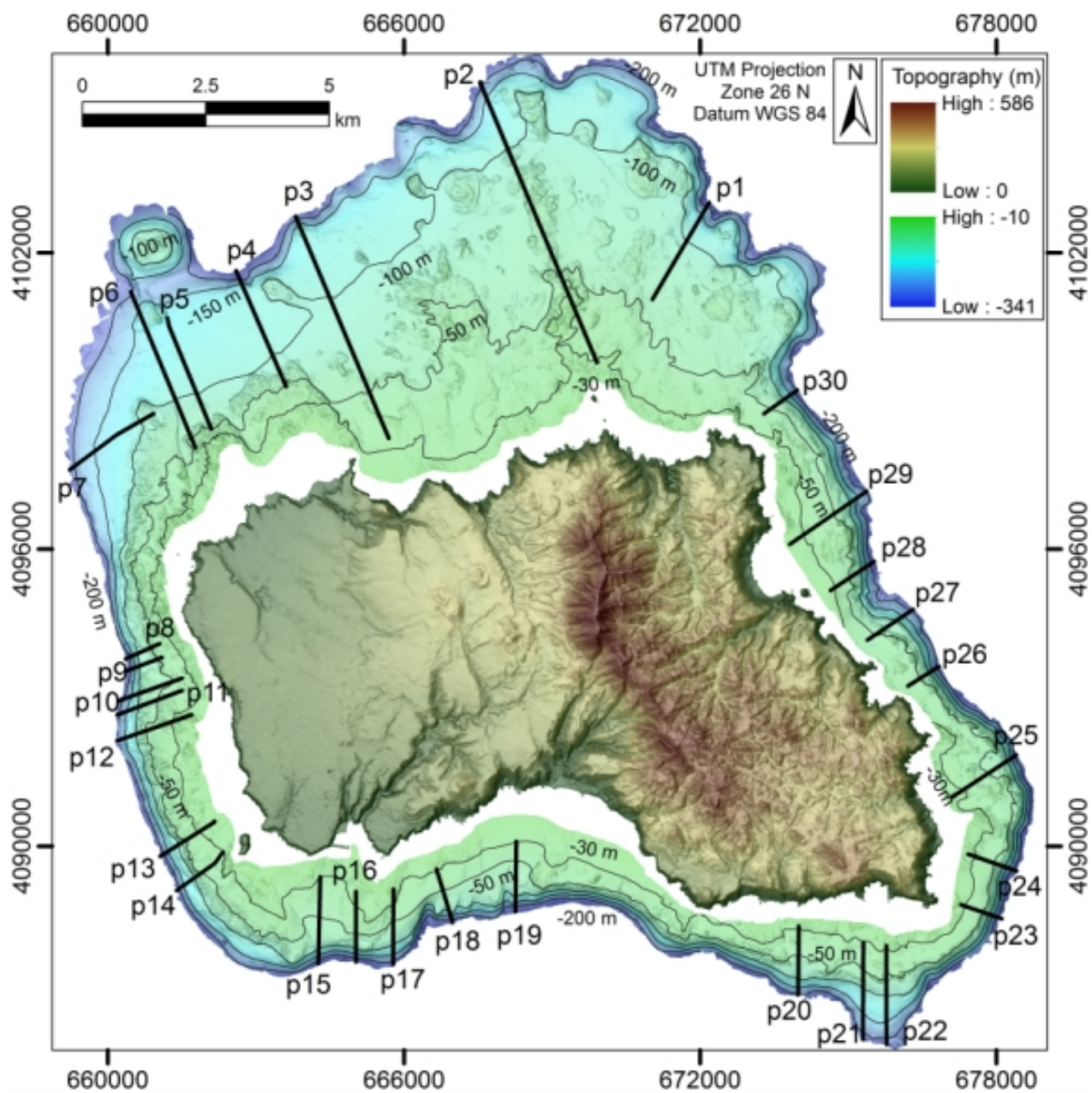105/110 m
120/125 m
140/145 m
155/165 m

Submerged terraces

-40/-50 m
-70/-80 m
-85/-90 m
-100/-110 m
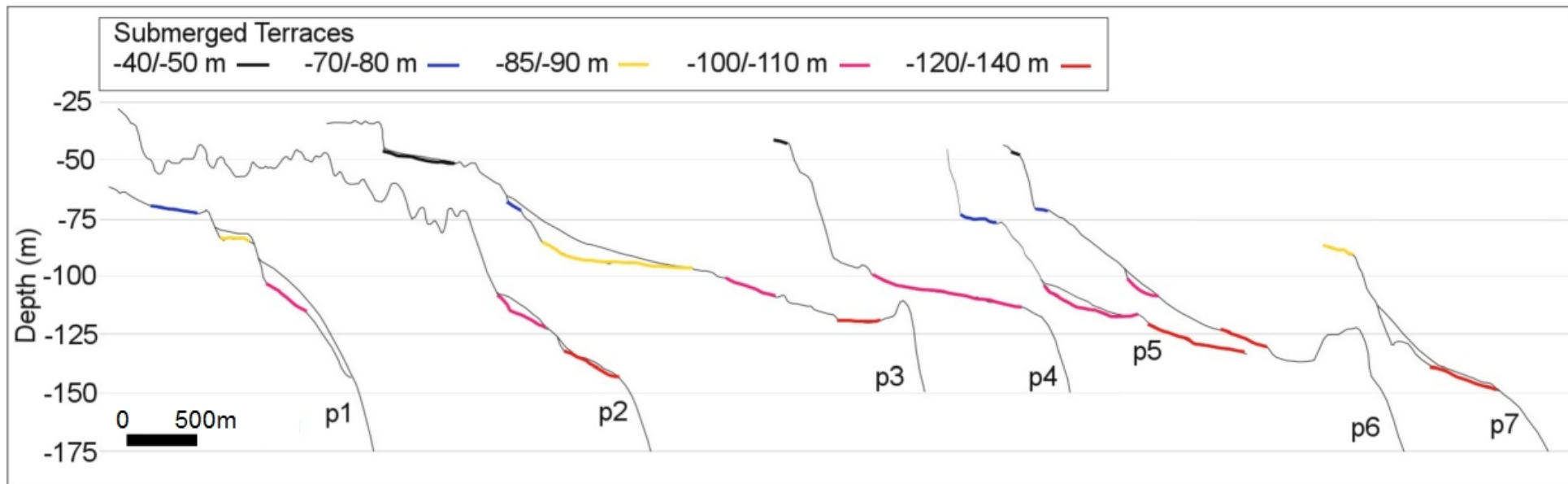-120/-140 m

Submerged terraces

Northern sector

Western sector

Southern sector

Eastern sector

ENE · Terrace inner margin · WSW

Submerged Terraces

-85/-90 m
-120/-140 m

Sediments

Erosive shelf edge

Depth (m)

100

150

200

0   250 m

SSE | NNW

Depth (m)

50 — 100 — 150

- Terrace inner margin

Submerged Terraces

-70/-80 m ——
-100/-110 m ——
-120/-140 m ——

Sediments

0   250 m

Submerged Terraces
-40/-50 m —— -70/-80 m —— -85/-90 m —— -100/-110 m —— -120/-140 m ——
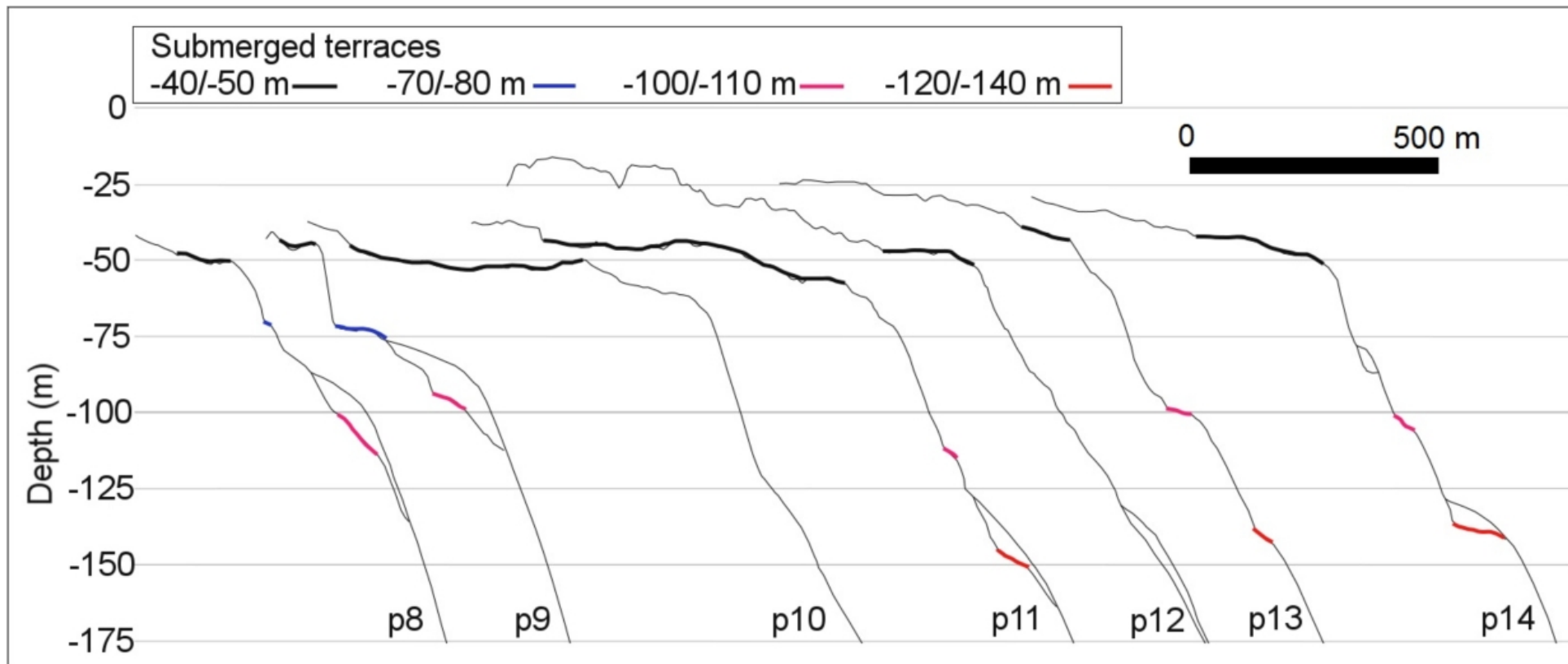
Submerged terraces
—40/-50 m —— -70/-80 m —— -85/-90 m ——

Submerged terraces	First passage (ka)	Last passage (ka)	Time span (ka)	Effective time (ka)
-40/-50m	1122	12.1	1109.9	197
-70/-80m	866	14	852	178
-85/-90m	642	14.7	627.3	65.6
-100/-110m	623	16.5	606.5	51.2
-120/-140m	19.8	19.8	0	8.7
Raised terraces				
7/11m	1749	121	1628	213.3
45/50	2525	1065	1460	305
55/60	2528	1425	1103	283.9
65/70	2598	1917	681	144.8
85/90	2717	2021	696	165.5
105/110	2809	2234	575	146.3
120/125	2818	2540	278	140.2
140/145	3145	2891	254	180.6
155/165	3436	3063	373	318.7

Table 1. Time of the first and last passage of sea level through the current depth/elevation of the inner margin of each marine terrace, according to sea-level fluctuations and the island uplift trend (see Fig. 15). Apart from the -120/-140 m terrace (possibly formed during a single lowstand), each marine terrace was likely carved and reworked several times within the overall time span reported in the third column (Time Span), resulting from the interval between the first and the last passage of the relative sea-level. The fourth column (Effective time) represents the time each terrace was effectively in the depth range (+/-5m) of sea level erosion within that time span, according to the adopted sea-level curves.

	Effective time (ka)	North (width)	West (width)	South (width)	East (width)
-40/-50	197	0.437 km	0.216 km	0.293 km	0.444 km
-70/-80	178	0.878 km	0.102 km	0.092 km	0.114 km
-85/-90	65.6	0.576 km	Absent	0.059 km	0.054 km
-100/-110	51.2	0.818 km	0.073 km	0.056 km	Absent
-120/-140	8.7	0.34 km	0.095 km	0.126 km	Absent

Table 2. Effective time the sea level was in the depth range of sea level erosion and width of respective submarine terraces for the northern, western, southern and eastern shelf sectors.

	Effective time (ka)	Width (m)
7/11 m	213.3	
45-50 m	305	450.25
55-60 m	283.9	400.75
65-70 m	144.8	344
85-90 m	165.5	299.75
105-110 m	146.3	405.25
120-125 m	140.2	290.25
140-145 m	180.6	120.5
155-165 m	318.7	276.5

Table 3. Effective time the sea level was in the depth range of sea level erosion and width of respective raised terraces.